



ANNUAL
REVIEWS **Further**

Click here to view this article's online features:

- Download figures as PPT slides
- Navigate linked references
- Download citations
- Explore related articles
- Search keywords

Physics of Ultrathin Films and Heterostructures of Rare-Earth Nickelates

S. Middey,¹ J. Chakhalian,¹ P. Mahadevan,²
J.W. Freeland,³ A.J. Millis,⁴ and D.D. Sarma⁵

¹Department of Physics, University of Arkansas, Fayetteville, Arkansas 72701;
email: smiddey@uark.edu, jchakhal@uark.edu

²S.N. Bose National Center for Basic Sciences, Salt Lake, Kolkata 700098, India;
email: priya@bose.res.in

³Advanced Photon Source, Argonne National Laboratory, Argonne, Illinois 60439;
email: freeland@anl.gov

⁴Department of Physics, Columbia University, New York, NY 10027;
email: millis@phys.columbia.edu

⁵Solid State and Structural Chemistry Unit, Indian Institute of Science, Bangalore 560012, India; email: sarma@sscu.iisc.ernet.in

Annu. Rev. Mater. Res. 2016. 46:305–34

First published online as a Review in Advance on April 6, 2016

The *Annual Review of Materials Research* is online at matsci.annualreviews.org

This article's doi:
10.1146/annurev-matsci-070115-032057

Copyright © 2016 by Annual Reviews.
All rights reserved

Keywords

correlated electrons, complex oxide heterostructures, metal-insulator transition, charge ordering, orbital engineering

Abstract

The electronic structure of transition metal oxides featuring correlated electrons can be rationalized within the Zaanen-Sawatzky-Allen framework. Following a brief description of the present paradigms of electronic behavior, we focus on the physics of rare-earth nickelates as an archetype of complexity emerging within the charge transfer regime. The intriguing prospect of realizing the physics of high- T_c cuprates through heterostructuring resulted in a massive endeavor to epitaxially stabilize these materials in ultrathin form. A plethora of new phenomena unfolded in such artificial structures due to the effect of epitaxial strain, quantum confinement, and interfacial charge transfer. Here we review the present status of artificial rare-earth nickelates in an effort to uncover the interconnection between the electronic and magnetic behavior and the underlying crystal structure. We conclude by discussing future directions to disentangle the puzzle regarding the origin of the metal-insulator transition, the role of oxygen holes, and the true nature of the antiferromagnetic spin configuration in the ultrathin limit.

U : electron-electron
Coulomb interaction
strength

Δ : charge transfer
energy

1. INTRODUCTION

Complex oxides consisting of transition metal ions offer a vast landscape of fascinating phenomena such as metal-insulator transitions (MITs), spin, charge and orbital orderings, high-temperature superconductivity, colossal magnetoresistance, and multiferroicity (1). The subtle competition between bandwidth (W), on-site electron-electron interaction strength (U), and charge transfer energy between oxygen and transition metal sites (Δ), together with the possibility of multiple oxidation states typically available to transition metal ions and a wide range of structural variations, results in an unprecedented diversity of interesting phenomena (2, 3). The quest to understand and control these phenomena has captured the imagination of generations of condensed matter physicists and has fostered the development of advanced experimental probes and theoretical methods.

Thin films and heterostructures add an important new dimension to the problem. Recent advances in atomic-precision oxide growth (4–8) enable new classes of materials to be created and studied. Behaviors exhibited by ultrathin films and heterointerface systems are different than in bulk, and the multiplicity of options for film growth and heterostructuring open new possibilities for control of material form and, thus, for controlled comparison of the relation between structure and properties. For example, growing films on different substrates lead to different strain states, and the materials respond with different degrees of octahedral tilts and rotations, resulting in different electronic properties. Similarly, quantum confinement and interfacial charge transfer can change the underlying physics.

In this review, we focus on the perovskite rare-earth nickelate compounds, with chemical formula $RENiO_3$, where $RE = \text{La, Pr, Nd, Sm, Eu} \dots \text{Lu}$. This material family exhibits rich physics, including charge ordering, strong electron-lattice coupling, MIT, and long-period magnetically ordered state, all controlled by the interplay of crystal structure and electron correlations. **Figure 1** schematically shows the rich diversity of ground-state properties and their relationship to different physical parameters that can be controlled via diverse experimental realizations.

A crucial issue in the material physics of complex oxides is orbital control: In a simple ionic picture, the Ni is in a low-spin d^7 state, with one electron in the twofold degenerate e_g orbitals. In bulk materials, the occupation probabilities of the two orbitals are nearly equal. An issue that has attracted some recent interest is the extent to which orbital engineering (a controllable differential occupancy of the e_g orbitals by changing strain and quantum confinement in ultrathin films) is possible. The issue is important both in the context of the nickelate materials and more generally as an example of control of many-body electronic structure. In this article, we review the known properties of the bulk $RENiO_3$ materials and then how these are modified in ultrathin film and heterostructured geometry.

2. CLASSIFICATION OF CORRELATED MATERIALS FROM AN ELECTRONIC STRUCTURE POINT OF VIEW

As these $RENiO_3$ are correlated oxides, we begin this review with a basic description of electronic structure parameters of such transition metal compounds. Efforts to classify the electronic structure of transition metal compounds started with attempts to understand why many of these have insulating ground states in spite of having partially filled d levels. Much attention has focused on NiO; the notional electronic configuration of the Ni^{2+} ion is $3d^8$ in the crystal field-split $t_{2g}^6 e_g^2$ configuration, with fully filled t_{2g} -derived bands and half-filled e_g -derived bands. One of the early suggestions due to Slater (9) emphasized the doubling of the unit cell due to the ground-state antiferromagnetic (AFM) order of NiO and the consequent opening of a gap in the half-filled e_g bands. A density functional theory (DFT)-based ab initio band structure calculation (10) indeed

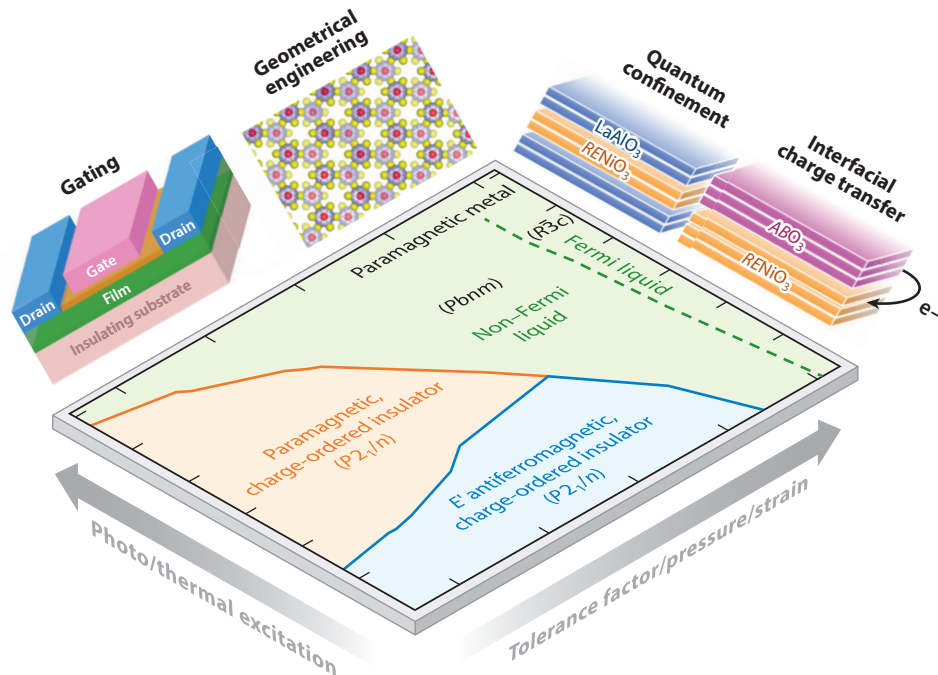


Figure 1

Bulk phase diagram of $RENiO_3$ and various experimental ways of altering these ground states, discussed in this review.

obtained a ground-state insulator for NiO. However, this approach is not entirely satisfactory, because the calculated band gap value is an order of magnitude smaller than the experimental value, and NiO continues to show insulating behavior above the Néel temperature.

Mott (11, 12) proposed an alternative idea that strong correlation effects in the d shell can lead to an insulating phase, even in a system with partially occupied levels. Hubbard (13, 14) analyzed a theoretical model based on Mott's ideas and showed that a sufficiently large on-site Coulomb interaction strength, U , within a partially occupied level can indeed localize electrons. The one-electron-removal spectrum, known as the lower Hubbard band (LHB) [corresponding to the occupied density of states (DOS) in a noninteracting system], is separated from the one-electron-addition spectrum, known as the upper Hubbard band (UHB) (corresponding to the unoccupied part of the DOS), shown in **Figure 2a**, when $U > U_c$, where U_c is in the order of the bandwidth (W) of the system dictated by the interatomic hopping interaction strength, t . Such a system is known as the Mott-Hubbard insulator, and its band gap is controlled primarily by the magnitude of U .

Fujimori & Minami's (15) analysis of spectroscopic features of NiO established the additional necessity of accounting explicitly for oxygen $2p$ levels because the primary hopping interaction t_{pd} in NiO connects O p and Ni d states. Achieving this requires the inclusion of an additional energy scale, Δ , needed to transfer an electron from the fully filled oxygen levels to a Ni $3d$ orbital. The presence of the O p band, arising from p - p hopping interactions between different oxygen sites, in a typical transition metal oxide is shown in **Figure 2a** for the $\Delta > U$ limit. In the opposite limit of $\Delta < U$, the energy ordering of O p states, the LHB, and the UHB are as shown in **Figure 2b** for charge transfer insulators (2), with the O p band appearing within the gap between the UHB

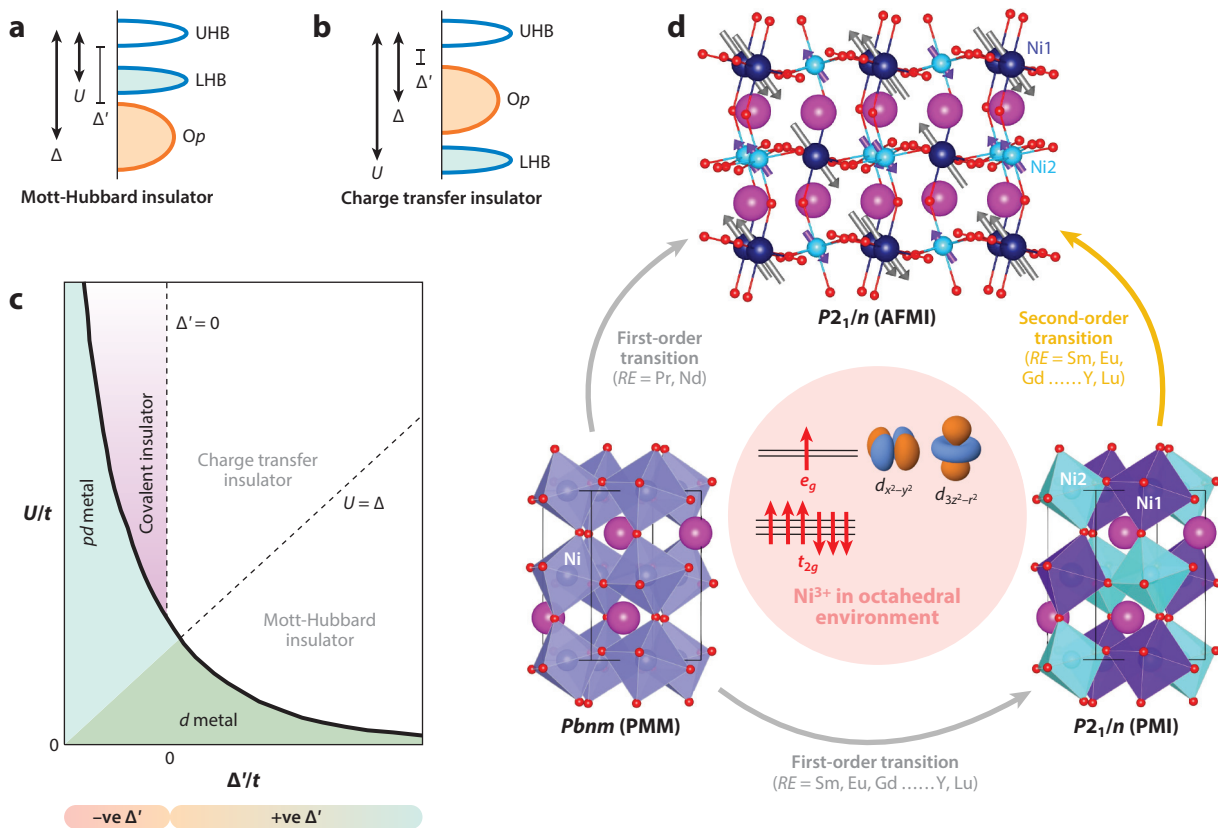


Figure 2

(a,b) Schematics of energy levels for (a) a Mott-Hubbard insulator and (b) a charge transfer insulator. (c) Modified Zaanen-Sawatzky-Allen phase diagram (2, 3). (d) Various transitions observed in bulk $RENiO_3$ series depending on the choice of RE ion. The electronic configuration of a Ni^{3+} ion is also shown for a pure ionic picture (d^7).

and the LHB. In this limit, the band gap, measured between the top of the O p band and the bottom of the UHB, is controlled more by Δ than by U , in contrast to the case for Mott-Hubbard insulators (**Figure 2a**). This scenario forms the basis of the name charge transfer insulator, as the lowest-energy excitation for charge transport is achieved here by transferring an O p electron to the transition metal d orbital.

Combining these ideas, Zaanen, Sawatzky & Allen (2) suggested that, instead of a single U_c as envisaged by Mott and Hubbard, the metallic and insulating ground states of transition metal compounds are separated by a line in the U - Δ phase space, with Mott-Hubbard insulators for $U_c < U < \Delta$ and charge transfer insulators for $U > \Delta > \Delta_c$. $3d$ orbitals contract across the $3d$ transition metal series, leading to a systematic increase in U (16). Within a related series of oxides, it is also known (17) that Δ decreases across the periodic table due to rapid stabilization of the $3d$ level with the increasing atomic number. This approach broadly categorizes insulating oxides of early $3d$ transition metals as Mott-Hubbard type, with larger Δ and lower U , and those of late $3d$ transition metals as charge transfer type, with smaller Δ and larger U .

For sufficiently small U , the system becomes metallic, as in Mott's description of the insulator-to-metal transition, due to the overlap of the top of the LHB with the bottom of the UHB.

Similarly, one would expect that, for a small enough Δ that makes the top of the O p band overlap the bottom of the UHB, defining the zero of the effective charge transfer energy, Δ' (see **Figure 2b**), the system will become metallic, as also suggested in the original Zaanen-Sawatzky-Allen phase diagram (2). However, it was later argued (18) that the insulating state will persist over a region of $\Delta' < 0$, depending on the value of t_{pd} and U , because t_{pd} will essentially mix the O p and metal d states, pushing them energetically apart to form a nonzero band gap, similar to the case of bonding-antibonding splitting formed in molecular orbital theory. This new region in the U - Δ phase space was termed the covalent insulating regime (18) to stress that the band gap originated from the presence of a sizable t_{pd} mixing O p and metal d states or covalency. This regime has also been referred to in the literature as the negative- Δ insulator (19, 20), although care should be taken to retain the distinction between Δ and the effective charge transfer energy, Δ' , in this context. Explicit calculations (3, 21) showed that this covalent insulator regime is increasingly stabilized with increasing t_{pd} and U . **Figure 2c** shows the resulting phase diagram, indicating different insulating and metallic regimes and establishing that the late transition metal oxides that are close to MITs—for example, many interesting Ni and Cu compounds, including the nickelates discussed in this review—belong to the covalent regime in their insulating state. Increasing the formal valence of a transition metal ion has the primary effect of lowering Δ and increasing t_{pd} . Thus, compounds of earlier transition metals, such as Co, Fe, Mn, and even Cr, may also be in the covalent insulating regime in their higher valence states. The correlation physics is different within the covalent insulating regime from the standard Mott paradigm due to the effective charge transfer energy being negative. One of the direct consequences of this negative effective charge transfer energy is that the ground-state wave function has a significant and often dominant contribution from the $d^{n+1}\underline{L}$ state, where n is the nominal d electron count and \underline{L} denotes a hole state generated in the ligand p orbitals. In contrast to the Mott limit, the dominant contribution arises from d^n states. In the case of nickelates with a formal d^7 configuration of Ni^{3+} , this ensures a significant contribution from the $d^8\underline{L}$ state in the ground-state wave function at the expense of the contribution from the d^7 states.

The above discussion suggests that localizing effects of increasing U and Δ are obviously important; however, the delocalizing effects arising from various hopping interactions as well as any other interaction—such as the crystal field and the spin-orbit interaction—that may influence bandwidth are also important and need to be treated on equal footing. This objective has been most successfully achieved through extensive developments of dynamical mean-field theory (DMFT), which provides the basis of most of our discussion of the electronic structure of nickelates in later sections of this review. At a simpler level of broad classifications, we already know from experimental studies that LaNiO_3 (LNO) is metallic, whereas all other members of the series, RENiO_3 , where RE is a rare-earth ion, are insulators at low temperature. Ab initio electronic structure calculations for the series RENiO_3 ($RE = \text{La, Pr, Nd, Sm, and Ho}$) (22) established a systematic reduction in the Ni d bandwidth by approximately 10% between La and Ho compounds. A fitting of the ab initio band dispersions to a minimal tight-binding model with Ni d and O p states did not show any substantial variation of t_{pd} across the series. The bandwidth reduction can, therefore, be related to the reduction of the hopping between different NiO_6 octahedra driven by a decreasing interoctahedral Ni-O-Ni angle with smaller RE ions across the series. Various features in the valence band photoemission spectra of LNO and NdNiO_3 (NNO) could be identified with features in the calculated DOS, underlining the importance of band structure effects (23, 24). An analysis of the $L_{23}M_{45}M_{45}$ Ni Auger spectrum revealed U of Ni to be 4.7 ± 0.5 eV. Hartree-Fock-type mean-field solutions of a multiband Hubbard model with these parameter strengths were found (23) to be consistent with LNO being metallic and NNO insulating.

3. COMPLEXITY IN BULK $RENiO_3$

Although we begin our discussion of ultrathin film nickelates by briefly reviewing several key phenomena present in the bulk counterpart, we refer the reader to the reviews by Medarde (25) and Catalan (26) for more details concerning bulk properties. Whereas the first member of the nickelate series, LNO with rhombohedral $R\bar{3}c$ structure, remains metallic down to the lowest temperature probed, the intermediate members with $RE = \text{Pr}$ and Nd undergo a first-order MIT from the paramagnetic metallic state with orthorhombic ($Pbnm$) structure to an antiferromagnetic insulating (AFI) state accompanied by a lowering of symmetry to monoclinic ($P2_1/n$). As the tolerance factor ($t = d_{RE-O} / \sqrt{2} d_{Ni-O}$, where d_{RE-O} and d_{Ni-O} are ionic bond distances between RE and O and between Ni and O, respectively) decreases further away from unity for even smaller RE ions (e.g., $\text{Sm} \dots \text{Lu}$), the MIT temperature (T_{MIT}) and magnetic transition (T_N) start to separate from each other (Figure 1). Within the insulating phase, the entire family has monoclinic ($P2_1/n$) structure (Figures 1 and 2c) with two inequivalent Ni sites in the unit cell.

Electrical and thermal measurements on the bulk and thin films revealed the signatures of complex multiband behavior (27), which has been further corroborated by angle-resolved photoemission spectroscopy (ARPES) measurement (28). Surprisingly, despite sharp changes in conductivity and lattice parameters across the MIT, optical conductivity measurements revealed only a gradual opening of band gap with continuous changes in spectral weight of the Drude peak (29). The reported optical gap of ~ 1 eV is also much larger than the gap (~ 20 meV) obtained from electrical conductivity data (30). Recent tunneling experiments showed the opening of a sharp gap (~ 30 meV) in the insulating state and the existence of a pseudogap in metallic LNO (31).

In the ionic picture, $RENiO_3$ compounds have NiO_6 octahedra with Ni^{3+} ions in the d^7 low-spin electronic configuration ($t_{2g}^6 e_g^1$; $S = 1/2$), which are expected to be Jahn-Teller active. However, resonant X-ray diffraction (RXD) experiments showed ordering of local magnetic moments on Ni sites in the AFI phase and ruled out any orbital ordering (32, 33). The magnetic ground state of these spins (Figure 2c) was initially deduced from neutron powder diffraction (34). The magnetic wave vector for the AFM state was determined to be $(1/2, 0, 1/2)_{ortho}$ [$(1/4, 1/4, 1/4)$ in the pseudocubic notation]; the spin arrangement of this E' AFM state can be viewed as a sequence of either $\uparrow\uparrow\downarrow\downarrow$ or $\uparrow\rightarrow\downarrow\leftarrow$ pseudocubic (111) planes, and the noncollinear spin scenario has been demonstrated by resonant X-ray scattering (35). Whereas two distinct magnetic moments, $1.4 \mu_B$ and $0.7 \mu_B$, consistent with a checkerboard-type charge ordering pattern were determined for $YNiO_3$ (36), the magnetic moments in the $RE = \text{Pr}$ (34, 37), Nd (34, 37), Sm (37, 38), and Eu (37, 38) compounds were found to be similar on each Ni site. This surprising result was further corroborated by RXD experiments in which a very similar energy dependence of magnetic scattering intensity was recorded across the series, with a similar spectroscopic signature for the local moment on Ni (39). In view of the strong variation of structural distortion and the magnitude of T_{MIT} in the $RENiO_3$ series, both measurements raised concern about the true nature of the charge ordering state. A view that aligns many of these facts is a picture in which the strong covalency leads the ground state to be more $3d^8\bar{L}$, and the charge ordering pattern in this picture resides not on Ni but on the oxygen site (i.e., $3d^8\bar{L} - 3d^8\bar{L} \rightarrow 3d^8 - 3d^8\bar{L}^2$) (40).

4. EPITAXIAL STABILIZATION

The +2 charge state is the most common oxidation state of Ni, and $RENiO_3$ requires Ni oxidation state to be +3. Such a high oxidation state is stabilized only under a high oxygen pressure $P \sim 200$ bar and an elevated temperature of $1,000^\circ\text{C}$ (41). Despite the extreme synthesis conditions, only micrometer-sized single crystals have been obtained for these nickelates (except for

LNO) (42), limiting the application of many experimental techniques crucial for understanding the underlying physics of these materials. As an alternate route, the growth of thin films is a feasible solution for obtaining large-size single-crystalline materials. Not surprisingly, many crucial pieces of information discussed in Section 3 were obtained by using single-crystalline thin films.

4.1. Thermodynamic Stability

Whereas thin films of LNO could be grown without high oxygen pressure by pulsed laser deposition (PLD) (43) and sputtering (44), stoichiometric NNO films with a bulk-like MIT were initially achieved only by postannealing under high oxygen pressure (~ 115 bar) (45). Later, epitaxial films for several members of the family were successfully synthesized at much reduced oxygen pressure (< 0.02 bar) by metal-organic chemical vapor deposition techniques by Novojilov et al. (46). Following this success, high-quality epitaxy at low oxygen partial pressure was also realized by PLD (47), sputtering (48), and all-oxide molecular beam epitaxy (49).

To understand how a single-crystalline phase can be obtained outside the thermodynamic phase diagram [$P(\text{O}_2)$ - T] of bulk materials, we consider the model of epitaxial stabilization of thin films (50). In this phenomenological framework, the relative difference between the free energies for the bulk and epitaxially stabilized phases is given by

$$\Delta E = \Delta E^{\text{ic}} - \Delta E^{\text{c}} = b \left[\Delta g_v^{\text{ic}} - \Delta g_v^{\text{c}} - \frac{\mu}{1-\nu} \epsilon^2 \right] + [\sigma_s^{\text{ic}} - \sigma_s^{\text{c}}]. \quad 1.$$

Here the superscripts c and ic denote the epitaxially coherent and incoherent (i.e., free from substrate) phases, respectively; b is the film thickness; Δg_v is the Gibbs free energy per unit volume; μ is the shear modulus; ν is Poisson's ratio; ϵ is the relative lattice mismatch between the unit cell parameters of the desired phase and the substrate; and σ_s is the surface tension. Whereas the volume contribution (the first term) is always negative, the surface contribution (the second term) is always positive. If the energy contributions are such that $\Delta E > 0$, then an epitaxially coherent phase is stabilized (50). As seen in Equation 1, a dramatic reduction in the contribution to the free energy comes from the coherent film/substrate interface, implying that $RENiO_3$ phases can be stabilized on a perovskite substrate whereas the films on nonperovskite substrates like MgO and ZrO_2 lack the required coherency and enforce the phase decomposition to $RENiO_3 \rightarrow REO_x + NiO$ (51). Moreover, as indicated by Equation 1, the increase of film thickness (b) as well as the larger lattice mismatch (ϵ) may further amplify the phase decomposition (i.e., RE_2O_3 and NiO) away from the single-phase perovskite film (46). Because the formation energy of $RENiO_3$ [$\Delta G_{RENiO_3} = \Delta G_{LaNiO_3} + (b - sT)(r_{RE^{3+}} - r_{La^{3+}} - \frac{1}{4}RT \ln(P))$] also increases with decreasing tolerance factor (52), the epitaxial stabilization of the distorted members of the series becomes much more difficult. In recent years, several groups have overcome this challenge and have successfully stabilized ultrathin films of $RENiO_3$ with $RE = \text{Pr, Nd, Sm, and Eu}$ (53–59).

4.2. Polarity Mismatch

The interest in nickelate heterostructures also brought to light the issue of polar discontinuity at the substrate/film interface that results in a diverging potential, which is compensated for in several ways, e.g., by electronic reconstruction, cationic intermixing, and oxygen vacancies (60). In a pure ionic model, because $RENiO_3$ consists of alternating $[REO]^{1+}$, $[NiO_2]^{1-}$ atomic planes along the pseudocubic (001) direction, this polarity issue was investigated by growing a [1-uc LNO/1-uc LAO] superlattice (SL) on nonpolar $SrTiO_3$ (STO) ($[SrO]^0$, $[TiO_2]^0$) and polar $LaAlO_3$ (LAO) ($[LaO]^{1+}$, $[AlO_2]^{1-}$) (uc denotes pseudocubic unit cell). Whereas the matched polarity on the

SL: superlattice

LAO substrate yields the desired +3 valence of Ni, the polar mismatched case of LNO on STO yields the first unit cell with Ni in the +2 oxidation state (61). Careful high-resolution transmission electron microscopy (HRTEM) combined with electron energy loss spectroscopy (EELS) confirmed $\text{Ni}^{2+}\text{O}^{2-}$ precipitation driven by the interfacial polar fields (62). This precipitation of the Ni^{2+} -containing layer can be suppressed by the careful growth of a buffer layer of LAO, which allows for the preservation of Ni^{3+} (61) in all nickel-containing layers. These experiments highlight the importance of taking into account the polarity mismatch in understanding material properties in heterostructures.

5. GROUND-STATE ENGINEERING THROUGH HETEROEPITAXY

Epitaxial stabilization on such a perovskite substrate not only provides the desired single-crystalline materials, but also allows ground-state engineering of nickelates by implementing the effect of, for example, strain, confinement, and charge transfer. This section discusses the recent rapid progress along these lines of research.

5.1. Epitaxial Strain in Ultrathin Films

Because epitaxial growth on a single-crystalline substrate forces the film to have the same in-plane lattice parameters during atom-on-atom growth, distortions, lattice symmetry, or octahedral tilts and rotations in the resulting thin film may become quite different from the bulk counterpart (63). Epitaxial strain is conventionally quantified by $\epsilon = (a_{\text{bulk}} - a_{\text{sub}})/a_{\text{bulk}}$, where a_{bulk} and a_{sub} are the pseudocubic lattice constants of bulk RENiO_3 and the substrate, respectively. However, as some chemical nonstoichiometry may be introduced during the growth, actual ϵ should be calculated using the experimentally measured lattice constant of an unstrained film (instead of a_{bulk}). The effect of strain on electronic and magnetic transitions of the RENiO_3 series has been thoroughly explored by diverse experimental probes, including thermal measurement and Hall effect measurement (58, 64, 65), synchrotron X-ray diffraction (66, 67), X-ray absorption spectroscopy (67–71), resonant soft-X-ray scattering (69, 72, 73), ARPES (74, 75), and optical spectroscopy (72, 76–78).

5.1.1. Orbital response to heteroepitaxy. Magnetic interactions in transition metal oxides are determined by the specific geometry of chemical bonds, the presence of various pathways for exchange interactions, the orbital configuration of the transition metal ions, and d electron occupancy. The strength and the nature (ferromagnetic versus AFM) of these exchange interactions can be summarized by the set of phenomenological rules, collectively known as Goodenough-Kanamori-Anderson rules, that reflect the strong intercoupling between spin, charge, and orbital degrees of freedom. On this basis, the fundamental step to employing heteroepitaxial engineering is to alter, via the orbital lattice interactions, the d -band orbital occupation and energy-level splittings caused by biaxial strain-induced lattice deformations. The orbital engineering in nickelates can be rationalized in the following way: Coherent heteroepitaxy imposes a tetragonal distortion on the film, thus removing the twofold e_g orbital degeneracy due to the distortion of the octahedral ligand field. Because both $d_{x^2-y^2}$ and $d_{3z^2-r^2}$ orbitals, constituting the degenerate e_g orbitals in an octahedral crystal field, have even symmetry, both tensile and compressive strains should symmetrically alter their energy positions relative to the strain-free energy band center. Although this symmetric strain-induced orbital polarization (SIOP) concept (**Figure 3a**) is a common view for rationalizing orbital responses, ultrathin films of many perovskite oxides surprisingly do not follow this simple notion (79).

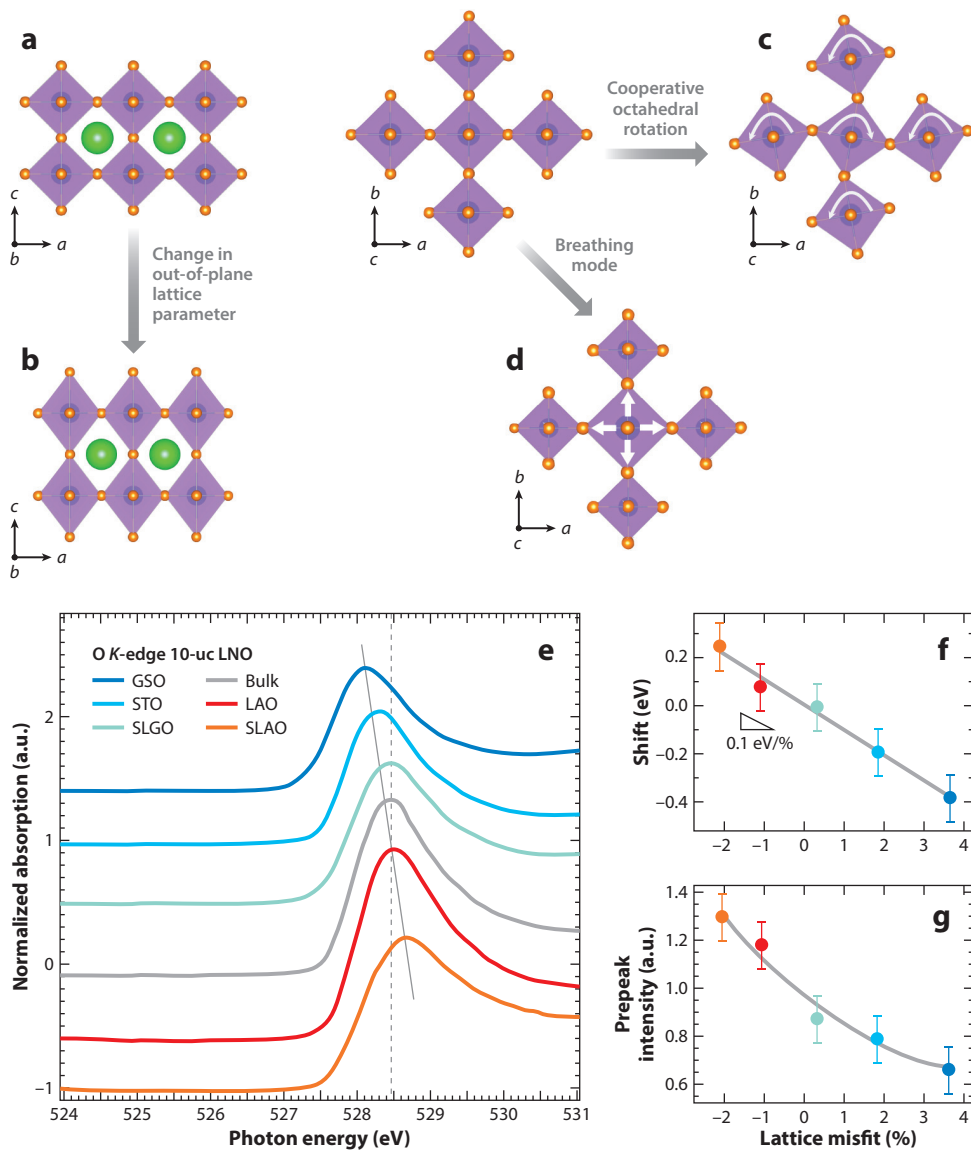


Figure 3

(a–d) Different types of distortions for accommodating lattice mismatch. (b) Out-of-plane expansion in an octahedron in accordance with the concept of symmetric strain-induced orbital polarization. (c) Cooperative octahedral rotation. (d) Breathing mode. (e–g) Effect of strain-induced change in Ni–O covalency for LNO: prepeak in O K-edge absorption for various strain states (e) and variation in (f) peak position and (g) normalized integrated intensity of the prepeak relative to bulk LNO with misfit ϵ . Abbreviations: GSO, GdScO₃; LAO, LaAlO₃; LNO, LaNiO₃; SLAO, SrLaAlO₄; SLGO, SrLaGaO₄; STO, SrTiO₃. Panels e–g adapted with permission from Reference 68. Copyright 2011, American Physical Society.

To understand how the SIOP model is violated, a 10-uc-thick film of LNO was grown on LAO ($\epsilon = -1.1\%$) and STO ($\epsilon = +1.8\%$) substrates (68). For the LAO case, X-ray linear dichroism (XLD) measurement showed a 100-meV lowering of the Ni $d_{3z^2-r^2}$ orbital compared to the $d_{x^2-y^2}$ orbital, confirming the compression of in-plane Ni-O bonds and enlargement of the out-of-plane (apical) Ni-O bonds—as expected from the SIOP model. Following the SIOP model, an inversion of the e_g orbitals was expected for tensile strain on STO. Surprisingly, no orbital polarization was detected for the STO case, although reciprocal space mapping confirmed that the film was fully coherent with in-plane lattice matched to the STO substrate (67, 68). This asymmetric orbital-lattice response to epitaxial strain signals the existence of alternative compensation mechanisms for strain accommodation (63, 80). DFT calculations with the experimentally determined lattice constants showed the existence of a single type of distorted NiO₆ octahedra with different in-plane and out-of-plane Ni-O bonds resulting in finite orbital polarization for compressive strain. In contrast, tensile strain was preferentially accommodated by cooperative octahedral rotations (**Figure 3b**) and breathing mode distortions (**Figure 3c**). The importance of these phonon modes is highlighted by the observation of breathing mode distortion that causes a Ni-O bond length disproportionation with alternating octahedra of Ni(1)O₆ (short Ni-O bonds) and Ni(2)O₆ (long Ni-O bonds), which are all equivalent in bulk LNO.

Further XLD experiments on NNO films revealed that, in contrast to LNO, under tensile strain the $d_{3z^2-r^2}$ orbital has a higher energy than does $d_{x^2-y^2}$ (67), as expected from the SIOP model for tensile strain. Such lifting of orbital degeneracy was also seen by hard-X-ray RIXS (resonant inelastic X-ray scattering) measurements, which identified a splitting of 0.4 eV between the e_g states (81). This markedly different response of LNO versus NNO was attributed to the difference in octahedral rotational pattern of bulk— $a^- a^- a^-$ (LNO) and $a^- a^- c^+$ (NNO) in Glazer notation—thus emphasizing the importance of lattice symmetry and how it interacts with strain-driven distortions of the structure (67).

5.1.2. Strain-induced self-doping. Because $RENiO_3$ belongs to a part of U - Δ phase space with an effectively negative charge transfer energy and a high degree of covalency, the ground state of $RENiO_3$ is a strong admixture of d^7 and $d^8\bar{L}$ electronic configurations (\bar{L} is a ligand hole on the oxygen p orbitals). This $d^8\bar{L}$ state manifests itself as a characteristic prepeak around 528.5 eV in O K -edge ($1s \rightarrow p$) X-ray absorption spectra (XAS). Due to the weak core-hole interaction, the O K -edge XAS is an approximate measure of oxygen projected unoccupied DOS (82), and the intensity, position, and width of the prepeak are markers of the degree of Ni-O bond covalency. As shown in **Figure 3e**, for a series of LNO films subjected to both tensile and compressive strain, the prepeak revealed a systematic evolution in the peak energy position with the imposed amount of epitaxial strain. The direct strain control of ligand-hole density was deduced from the nearly linear dependence of the peak position with ϵ (**Figure 3f**). The charge transfer energy $\Delta = e\delta V_{\text{Mad}} + I(\text{O}^{2-}) - A(M^{v+}) - e^2/d_{M-\text{O}}$ in the ionic model (1)—where $I(\text{O}^{2-})$ is the ionization potential of oxygen, $A(M^{v+})$ is the electron affinity of transition metal ion M^{v+} , and $d_{M-\text{O}}$ is the nearest-neighbor metal-oxygen distance—depends on the relative Madelung potential δV_{Mad} between Ni and O, so the movement of the prepeak highlights a decrease in Δ with compressive strain. The corresponding decrease in full width at half-maximum (FWHM) with increasing tensile strain (**Figure 3g**) implies the narrowing of electron bandwidth (W). The strong modulation in both Δ and W implies a strain-induced unusual self-doping effect, which was further substantiated by temperature-dependent Hall coefficient and thermoelectric power measurements (65).

5.1.3. Strain-driven phase engineering. As the nature of the ground states and the transition temperatures depend strongly of Ni-O-Ni bond angle and Ni-O bond length, epitaxial strain is

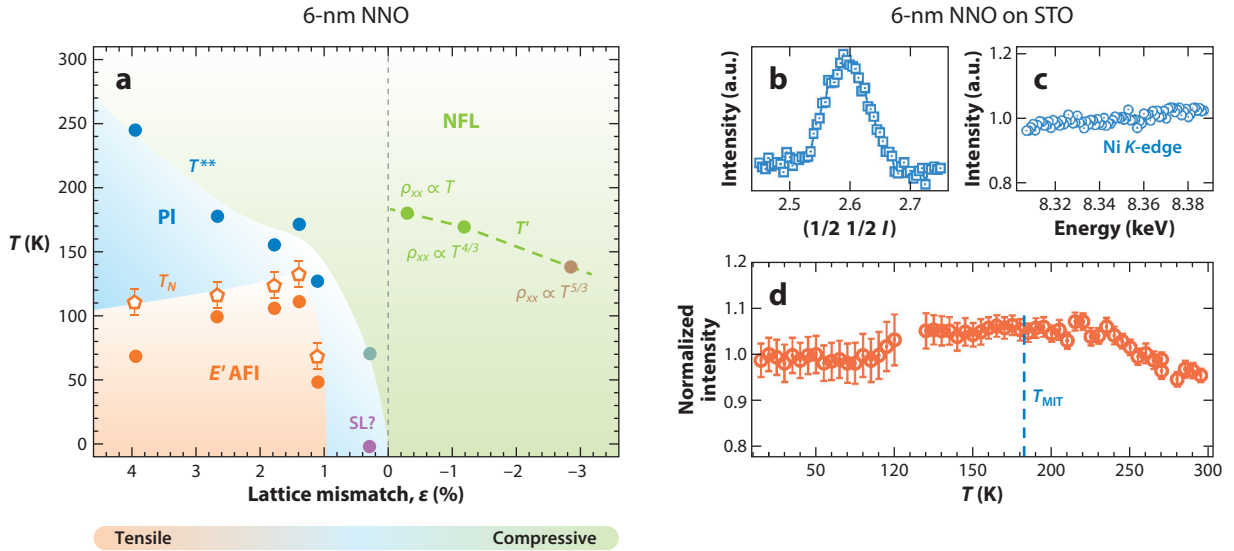


Figure 4

(a) Lattice mismatch-temperature phase diagram for 6-nm thin NNO film. Panel *a* adapted from Reference 69. T^{**} (blue), T_0 (green), and the hysteric inflection point (orange) are denoted by closed circles, whereas T_N is denoted by the open pentagons, and its error bar is defined as the temperature step size, 10 K. (b) l scan through $(1/2\ 1/2\ 5/2)_{pc}$ reflection for NNO on a STO substrate. Due to the twinned domain structure of the film, this reflection is a combination of $(105)_{ortho}$, $(015)_{ortho}$, $(231)_{ortho}$, and $(321)_{ortho}$ reflections. (c) Ni does not contribute to this reflection even in the insulating phase, as demonstrated by the energy scan around the Ni K -edge. (d) Temperature dependence of this reflection, recorded during the heating run from low temperature. For details of panels *b*–*d*, see Reference 81. The absence of Ni contribution to the $(b0l)_{ortho}$ reflection with odd b and l in such ultrathin films was also confirmed for a single-domain NNO film grown on a NdGaO_3 substrate (90). Abbreviations: AFI, antiferromagnetic insulator; NFL, non-Fermi liquid; NNO, NdNiO_3 ; pc, pseudocubic; PI, paramagnetic insulator; SL, superlattice; STO, SrTiO_3 .

expected to have a profound impact on the electronic and magnetic properties. To investigate this possibility, Liu et al. (56, 69) investigated 6-nm NNO films as a function of epitaxial strain. The result shown in **Figure 4a** indicates that, unlike for the bulk, where $T_{MIT} = T_N$, the transitions get separated, with the degree of separation scaling with the tensile strain. On the compressive side, temperature-induced MIT is completely quenched. Although several reports (46, 83–85) revealed the preservation of the MIT in compressively strained films, a recent study by Hauser et al. (58) demonstrated that those films are actually partially relaxed, and optimally prepared films under compressive strain are entirely metallic (58, 86), consistent with the reports of Liu and coworkers (56, 69). Liu et al. found that the resistivity of this anomalous metallic state exhibits non-Fermi liquid (NFL) behavior in the vicinity of a quantum critical point akin to the case of bulk PrNiO_3 under external pressure (87, 88). From those observations, it was concluded that film behavior under increasing tensile strain resembles the A -site replacement by a smaller RE ion of the bulk, whereas the effect of compressive strain is very similar to that of hydrostatic pressure. The exponent of the NFL phase is also not affected by the change of film thickness (86). Although resistance of these films surpasses the Mott-Ioffe-Regel limit at high temperatures (89), unlike the case for the cuprates ρ eventually saturates for nickelates. The value of this saturation resistance is related to the orbital splitting between $d_{x^2-y^2}$ and $d_{3z^2-r^2}$ orbitals (86). The effect of epitaxial strain was also investigated for the distorted $RENiO_3$ members with $T_{MIT} > T_N$ (70, 71, 73). Similar to the NNO case, the separation between T_{MIT} and T_N decreases as the amount of tensile strain is lowered and the films grown under large compressive strain become entirely metallic (73).

5.1.4. Selective suppression of order parameters through epitaxy. Although both the AFM order and the MIT are preserved in epitaxially grown NNO films with $\epsilon > +1.1\%$, the next important question is whether the proximity to the substrate of different crystal symmetry can alter the orthorhombic-to-monoclinic symmetry lowering across the MIT and the concomitant charge ordering. The charge ordering scenario in bulk-like NNO films was investigated with resonant X-ray scattering experiments at the Ni K -edge (91). In the high-symmetry orthorhombic metallic phase, Ni sites do not contribute to particular reflections, which gain a Ni contribution in the low-temperature monoclinic phase and can be used to study the details of the charge ordering phase via the resonant signature (32, 91, 92). An interesting recent result is that, for an ultrathin (6-nm) NNO film grown under tensile strain, even though the film displayed an MIT and magnetic ordering, there was no resonant Ni signal for these reflections, even in the insulating phase (**Figure 4c**). This observation, together with the absence of any detectable temperature dependence of the reflection (**Figure 4d**), led to the conclusion that $Pbmm$ symmetry is preserved deep into the insulating state (81, 90). This result implies the exceptionally rare case of a purely electronic Mott-Hubbard MIT that is driven by magnetic ordering.

Despite the absence of both a lattice symmetry change and Ni charge disproportionation, the transition was accompanied by a peculiar charge redistribution from Ni $3d$ to Nd $5d$ orbitals that may play a role in the MIT (81). Although the relevance of the Mott-Hubbard picture of the nature of the MIT was highlighted by the midgap spectral weight transfer in optics measurements (76), the charge redistribution, which involves the A -site states, questions the simple picture of the conventional Mott transition. The K -edge RIXS measurement and the resonant X-ray scattering data suggest that the MIT is neither pure Mott-Hubbard nor pure charge transfer.

In contrast to the case for NNO, the bulk-like charge ordering pattern remains unaltered in ultrathin films of highly distorted EuNiO_3 (93). Those experiments stress the exquisite sensitivity of the electronic structure in the insulating state to various types of structural distortions (94), including the Jahn-Teller distortion (NNO) and breathing mode distortion (EuNiO_3), under epitaxial constraint. The issue of charge ordering in such geometry was also investigated by Raman scattering (72), and phonon modes characteristic of the charge ordering were indeed observed in the insulating state of thin films and SLs of PrNiO_3 (of thickness ~ 12 nm) under tensile strain. Interestingly, these Raman modes were absent in SLs under compressive strain, which are weakly metallic but retain E' AFM ordering. Such an AFM metallic phase does not exist in the bulk nickelate and has been referred to as a spin-density wave phase (72), which was predicted theoretically by Lee and coworkers (95, 96).

5.2. Quantum Confinement in Heterostructures

The ability to grow these materials with sub-unit cell precision has opened another new dimension to explore highly two-dimensional electronic and magnetic phases in the quantum confinement regime. The SL structure, which consists of an electronically active material and a wide-band-gap insulator (for which one side can be vacuum), blocks electron hopping along the confining direction (i.e., across the interface); the specific choice of confining interface further determines the boundary condition in this quantum well geometry. In this section, we explore how heterostructures can be used to tune the electronic and magnetic states of nickelates.

5.2.1. Dimensionality and carrier localization. The correlated metallic behavior of bulk LNO provides a perfect playground to test the itinerant behavior of d electrons down to the atomic scale. Toward this goal, several groups explored the effect of dimensionality along with electron-electron correlations by growing a series of single-layer films and SL structures of LNO of different

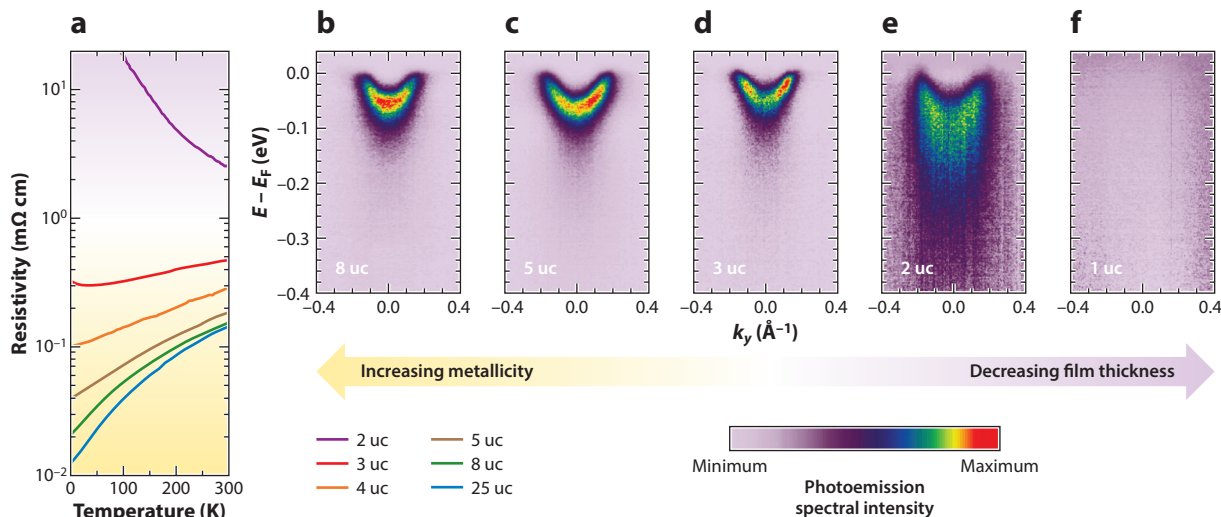


Figure 5

(a) MITs as a function of LNO layer thickness. (b–f) The evolution of electronic structures across the MIT is probed by angle-resolved spectroscopy along $(0.5 \pi/a, k_y, 0.7 \pi/a)$. Abbreviations: LNO, LaNiO₃; MIT, metal-insulator transition. Adapted with permission from Reference 75. Copyright 2014, Macmillan.

thicknesses (48, 75, 97–101). As an example, consider the results in **Figure 5a**, showing the temperature-dependent resistivity behavior for a series of LNO films grown on LAO substrates by oxide molecular beam epitaxy (75). Although the room temperature conductivity decreases with decreasing film thickness, the metallicity over the entire temperature range is maintained down to 4 uc. Upon approaching the 2-uc limit, the LNO film becomes insulating. Although all groups reported this confinement-induced MIT, the critical film thickness at which the insulating behavior sets in is strongly dependent on the strain value and the architecture (i.e., film versus SL). With respect to dimensionality effects in single-layer films, one issue is the presence (or lack) of a polar discontinuity, which may explain the differences in the results for LAO (75) versus STO (97). Resonant X-ray absorption spectroscopic measurements on Ni $L_{3,2}$ -edge complemented by first-principle calculation (98) and soft- and hard-X-ray photoemission spectroscopic measurements (100, 102) revealed a gradual evolution of electronic structure, including the charge transfer gap. X-ray diffraction showed a change in atomic arrangement in terms of both decreased Ni-O-Ni bond angle and lattice rumpling near the interface with a reduced number of unit cells (101). In addition, layer-resolved studies established that the suppression of DOS is more pronounced near the interface (103), where the octahedral tilts are larger than in the layers away from the interface (101, 104). All these results indicate that bandwidth control is an important component for the MIT as is the case for bulk nickelates (25, 26).

Recent ARPES studies (75) revealed the retention of bulk-like electronic structure and Fermi liquid characteristics (see the narrow parabolic band in **Figure 5b–d**) down to 3-uc thin film. The thickness-dependent MIT was attributed to the presence of a spin/charge instability in two dimensions (75).

5.2.2. Magnetism in confined architectures. Because all bulk *RE* nickelates that display a MIT also undergo magnetic transition, the observation of the insulating state in the few-unit-cell limit prompted several groups to investigate its spin degree of freedom. Ultrathin SLs were initially

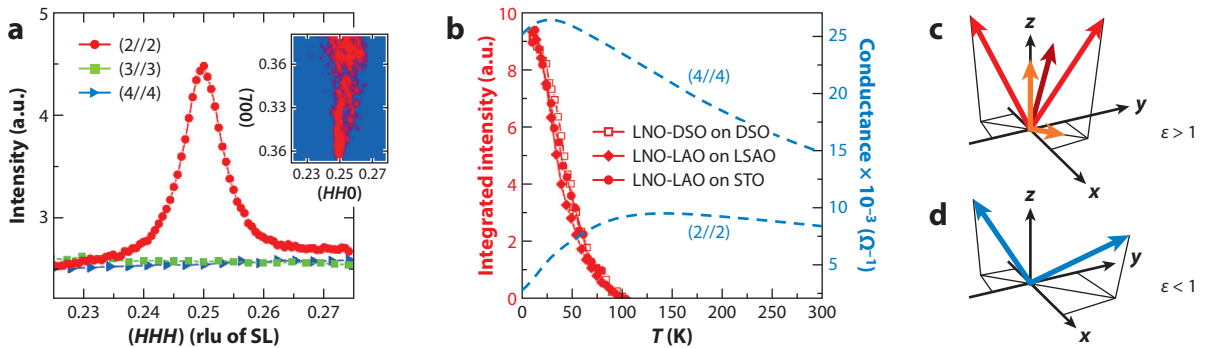
investigated by muon spin rotation (μ SR) (99), and metallic 4-uc LNO/4-uc LAO SLs were found to remain paramagnetic down to the lowest temperatures, as for the case of bulk LNO, but antiferromagnetism was clearly detected in the insulating phase of a 2-uc LNO/2-uc LAO SL. Because μ SR cannot determine the ordering pattern, a series of LNO SLs with dielectric spacers were grown on several substrates and were investigated by resonant soft-X-ray diffraction (105). **Figure 6a** shows the resulting L scans around $(1/4\ 1/4\ 1/4)_{\text{pc}}$ (where the subscripted pc denotes pseudocubic) $[(1/2\ 0\ 1/2)$ in the orthorhombic setting] with the incident photon energy tuned to the Ni L_3 -edge for N -uc LNO/ N -uc ABO_3 SLs with $N=2, 3, 4$ and $ABO_3 = \text{LaAlO}_3, \text{DyScO}_3$. The experiment clearly established the presence of bulk-like E' -type AFM order for all SLs with $N=2$. The strong dependence of spin direction on underlying structure obtained from the analysis of polarization dependence and azimuthal scans (**Figure 6c,d**) further emphasized the importance of spin-phonon coupling. Because this noncollinear AFM structure has the same propagation wave vector as the Fermi surface nesting vector obtained from calculations and the high-temperature phase is metallic (**Figure 6b**), this magnetic state has been interpreted as a spin-density wave. The disappearance of the spin-density-wave states for $N=3, 4$ SLs was attributed to the increasing three-dimensional Fermi surface that in turn suppresses the tendency for nesting together with the onset of the metallic phase. Such a nesting-driven mechanism behind magnetic ordering was further corroborated by very recent ARPES measurements (106). Similar polarization-dependent magnetic scattering experiments with azimuthal scans for thin films spanning the whole $RENiO_3$ series are necessary to probe any variation in the spin orientation with the change in the Ni-O-Ni bond angles.

5.2.3. Orbital polarization. From the electronic structure standpoint, due to the strong similarity between $RENiO_3$ and high- T_c cuprates (i.e., one electron versus one hole on the e_g orbital), Chaloupka & Khaliullin (109) proposed, as an analog to high- T_c superconductors, a single-unit-cell LNO layer heterostructured with a band insulator. In their model, it was assumed that tensile strain would enforce the electron into the $d_{x^2-y^2}$ state and that the insulating barrier across the interface would reduce the bandwidth of the $d_{3z^2-r^2}$ band by blocking the out-of-plane hopping. More recent local density approximation (LDA) + DMFT calculations corroborated the possibility of a cuprate-like Fermi surface in such heterojunctions (110).

This theory proposal sparked a vivid interest in orbital physics of $RENiO_3$ compounds. In addition to strain and quantum confinement, the choice of non-transition metal ion X in the LNO/LaXO₃ heterostructure was an important factor in controlling the degree of orbital polarization (111). Recall that, in the bulk, ligand holes are equally distributed over the 6-oxygen surrounding a central Ni ion. In the LNO/LaXO₃ SL, because of the strong ionic nature of X , the holes initially located on the apical oxygen (i.e., the Ni-O- X bond) would be redistributed back into the ab plane. This redistribution of holes would be akin to d -band filling having a strong effect on the d -orbital occupancy, altering the magnitude and even switching the sign of orbital polarization (111). After the charge transfer physics between Ni d states and O p states was explicitly incorporated into DFT + DMFT calculations, the resulting orbital polarization became considerably reduced (112).

The experimental work on orbital response to confinement and epitaxial strain revealed behavior that is significantly more complex than anticipated from the theory. For example, 1-uc LNO/1-uc LAO SLs grown under compressive strain on LAO showed equal electronic population of $d_{x^2-y^2}$ and $d_{3z^2-r^2}$ orbitals, even though the orbitals showed an energy splitting of ~ 100 meV (113). Disa et al. (114) also recently confirmed this zero orbital polarization. In contrast, the same SL grown under tensile strain on STO showed only $\sim 5\%$ orbital polarization and, most importantly, no splitting between the e_g orbitals. Ab initio calculations (113, 115) found that

Spin response to confinement and strain



Orbital response to confinement and strain

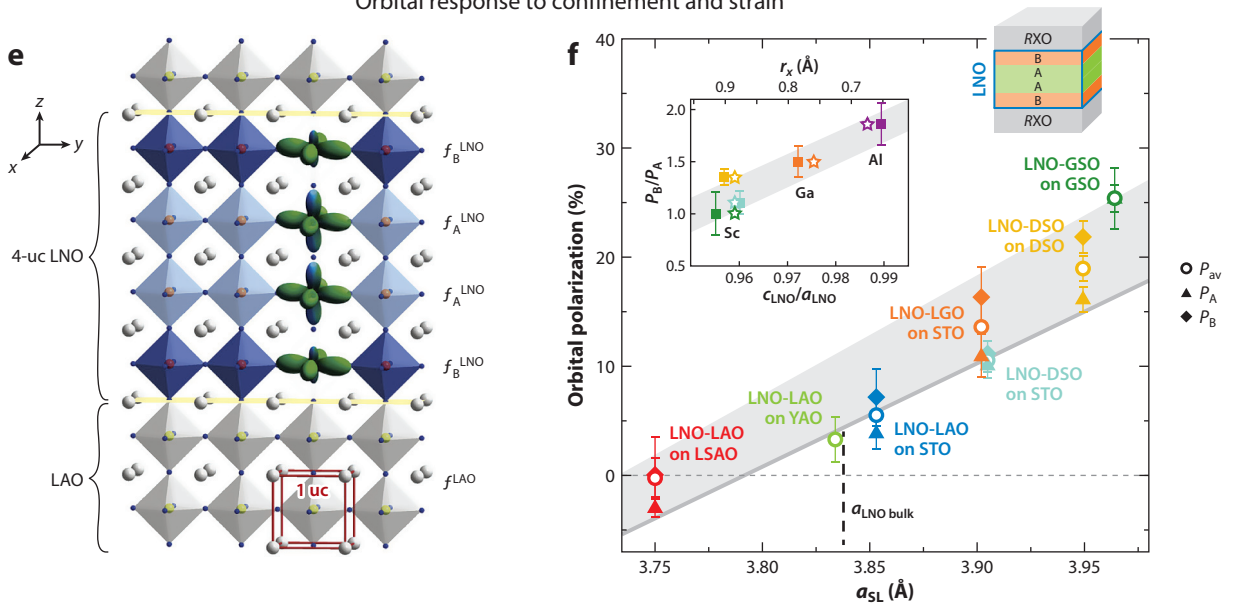


Figure 6

(a–d) Effect of confinement and epitaxial strain on Ni spins. (a) L scans around $q_0 = (1/4 \ 1/4 \ 1/4)_{\text{pc}}$ at 10 K and $E = 853.4$ eV for N -uc LNO/ N -uc ABO SLs ($ABO = \text{LAO, DSO}$). Reciprocal-space map of the scattered intensity of an $N = 2$ SL. (b) Temperature dependence of the magnetic Bragg intensity at q_0 for LNO-based SLs with $N = 2$ emphasizes a paramagnetic-to-antiferromagnetic transition. dc electrical conductance measurements for $N = 2$ and $N = 4$ SLs are also shown. (c) Spin directions of $N = 2$ SL under tensile strain. Red arrows (equal moments on each site are symmetrically tilted from the $[001]$ axis by $28 \pm 2^\circ$) and orange arrows (two spin sublattices: a large moment along $[001]$ and a small moment along $[110]$) show two possible arrangements. (d) The magnetic moments for $N = 2$ SL under compressive strain are similar to those of the bulk (33). (e) Schematic structure to highlight different orbital configurations of the interfacial layer compared with the orbital configurations of the bulk-like layers. (f) Orbital polarization as a function of substrate lattice parameter for various LNO-based superlattices. Abbreviations: DSO, DyScO_3 ; GSO, GdScO_3 ; LAO, LaAlO_3 ; LGO, LaGaO_4 ; LNO, LaNiO_3 ; LSAO, LaSrAlO_4 ; pc, pseudocubic; SL, superlattice; STO, SrTiO_3 ; YAO, YAlO_3 . Panels a–d adapted with permission from Reference 105. Copyright 2013, American Physical Society. Panel e adapted with permission from Reference 107. Copyright 2011, Macmillan. Panel f adapted with permission from Reference 108. Copyright 2013, American Physical Society.

the coordination between the Al and the Ni resulted in a chemical mismatch that influenced the hole density on the apical oxygen and subsequently the Ni $d_{3z^2-r^2}$ orbital. A new approach termed orbital reflectometry (a combined analysis of XLD and resonant X-ray reflectivity) (107) applied to a 4-uc LNO/4-uc LAO SL on a STO substrate also detected a similar value of the orbital polarization. As illustrated in **Figure 6c**, the power of this method is the ability to differentiate the orbital polarization across the layers. By careful choice of spacer layers and application of high tensile strain, large orbital polarization (up to 25%) was reported for a 4-uc LNO/4-uc GdScO₃ SL (108) (**Figure 6d**). A very recent study of a 4-uc PrNiO₃/4-uc PrAlO₃ SL revealed the presence of a smaller orbital polarization (P_{av}) of $\sim 5\%$ (116), which also decreases across the MIT. Interestingly, no significant temperature dependence of P_{av} was observed across the magnetic transition of compressively strained SLs, which had earlier been assigned as a spin-density wave phase (72).

5.3. Interfacial Charge Transfer

The redistribution of charge at the interface between two dissimilar materials is one of the key concepts behind modern electronics. The difference in the chemical potential may cause charge transfer across the interface. Such charge transfer in turn can alter spin and orbital sectors, resulting in novel electronic and magnetic states emerging in complex oxide heterostructures (5–8). For example, electronic reconstructions have been explored for LNO by forming an interface with manganites (117–122) and titanates (114, 123, 124).

Although bulk CaMnO₃ (CMO) is an AFM insulator, interfacial ferromagnetism limited within one unit cell of CMO from the interface was uncovered in N -uc CMO/ M -uc LNO SLs when the thickness ($M \geq 4$) was sufficient to make the system metallic (120). Because no sizable charge transfer was observed, the origin of ferromagnetism connected to the appearance of metallicity was attributed to double exchange between Mn⁴⁺ and Ni³⁺ along the interface. A ferromagnetic coupling between the interfacial layers was also explored in 2-uc LaMn³⁺O₃/ N -uc LaNi³⁺O₃ SLs, in which electron transfer from Mn to Ni led to the formation of a Mn⁴⁺-Ni²⁺ pair (119). In addition, a helical magnetic state without any spin-orbit coupling or Dzyaloshinskii-Moriya interaction emerging from this interfacial charge transfer in LNO layers was recently reported (125). When prepared along the [111] direction, LNO/LaMnO₃ SLs also displayed exchange bias, which was not seen for the [001]-oriented case (118).

As a way to engineer electronic correlations, an interface between Mott insulator LaTi³⁺O₃ and correlated metal LNO was recently proposed (123). The follow-up experiments confirmed that such a heterojunction exhibits massive interfacial charge transfer from Ti to Ni sites, resulting in an overall insulating ground state with a charge excitation gap of 0.2 eV between Ni d and Ti d states. The correlated gap between UHBs and LHBs for Ni was determined to be 1.5 eV (123, 124). After inserting extra LaTiO₃ layers into a single-unit-cell LNO/LAO heterostructure, an unusually high degree of orbital polarization ($\sim 50\%$) on Ni sites was reported and connected to the charge transfer between Ti and Ni (114, 126).

5.4. Geometrical Engineering

All films and heterostructures described above were synthesized along the pseudocubic [001] direction. Whereas along the [001]_{pc} direction ABO_3 consists of alternating AO and BO_2 atomic planes, the same perovskite along the [111]_{pc} direction consists of alternating $[AO_3]$ and B planes. Thus, by growing two pseudocubic unit cells of ABO_3 along [111]_{pc}, one can generate a new lattice with two vertically shifted triangular planes of B sites (**Figure 7a**). As illustrated in **Figure 7b**,

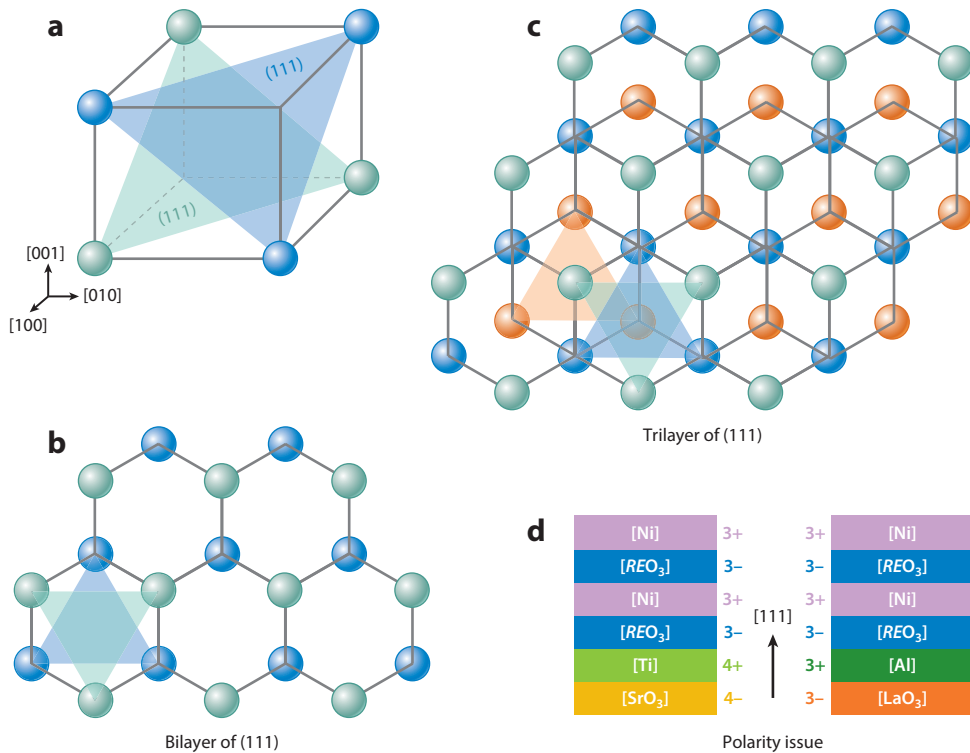


Figure 7

(a) (111) planes of *B* sites for an ABO_3 perovskite structure. (b,c) Bilayer (b) and trilayer (c) of such (111) planes generate a buckled honeycomb lattice and a dice lattice, respectively. For visual clarity, *A* and oxygen sites are not shown. (d) Schematics of polar discontinuity (in an ionic picture and without considering any surface reconstruction) for the growth of $RENiO_3$ on STO and LAO (111) substrates. Abbreviations: LAO, $LaAlO_3$; STO, $SrTiO_3$.

this artificially generated buckled honeycomb lattice provides a unique opportunity to investigate physics of *d* electrons in graphene-like geometry (127–129). Similarly, the dice lattice shown in **Figure 7c** can be obtained by growing 3 unit cells along the $[111]_{pc}$ direction (130).

Due to the difference in periodic arrangements of atoms along $[111]$ versus $[001]$, the theoretical calculations (128, 129, 131–133) for $[111]$ -oriented bilayers of nickelates have predicted the realization of several exotic phases unattainable in either bulk or (001)-oriented heterojunctions. For example, the model Hamiltonian calculations in the strongly correlated limit predicted that orbital ordering wins spontaneously over the bulk-like charge-ordered phase (128, 131–133), whereas in the weakly correlated limit, a number of topological phases (e.g., Dirac half-metal phase, quantum anomalous Hall insulator phase, and spin nematic phase) driven exclusively by interactions and without spin-orbit coupling were predicted (128, 129).

Because all popular perovskite substrates, including STO, LAO, $NdGaO_3$, and $YAlO_3$, are polar along $[111]$ with alternating $+4e$, $-4e$ (or $+3e$, $-3e$) charges per plane, epitaxial thin-film growth along this direction is rather undeveloped due to the possibility of complex structural, chemical, and electronic reconstructions that compensate for the polarity jump. To elucidate the issue, unit-cell-by-unit-cell growth was investigated by monitoring the growth progression with in situ reflection high-energy electron diffraction (RHEED) of LNO on STO (polar interface)

and LAO (nonpolar interface) (111) substrates (134). The measurements showed the presence of nonperovskite phases within the first 5 unit cells on the STO substrate; a combination of X-ray diffraction and resonant X-ray spectroscopy identified the formation of the $\text{La}_2\text{Ni}_2\text{O}_5$ phase. In contrast, stoichiometric LNO was successfully grown on a LAO (111) substrate, thus confirming that the absence of the polar mismatch at the interface is the key for quality [111]-oriented heterostructures (135).

Followed by the theoretical prediction (128, 129, 131–133), the behavior of d^7 Mott electrons on the honeycomb lattice was investigated by growing 2-uc NNO/4-uc LAO SLs on a LAO (111) substrate. The resultant system exhibits a new ground state characterized by AFM correlations and orbital ordering, and this lattice geometry-stabilized new ground state is unattainable in either bulk NNO or analogous heterostructures grown along the conventional [001] direction (136). Although design of *RE* nickelates with new lattice geometries is still in its infancy, the potential of this interesting concept for ground-state engineering was recently highlighted by a report of markedly larger charge transfer in *n* LNO/*n* LMO (111) SLs with $n=5, 7$ relative to the equivalent (001) SLs (122).

6. THEORETICAL UNDERSTANDING

The most important task of the theory of *RE* nickelates is to link the atomic physics of the strongly correlated Ni *d* orbitals to the behavior of actual materials. Issues of current importance include the nature of the MIT and its connection to lattice distortions and to magnetic ordering, the degree to which orbital occupancy can be varied by strain or other external parameters, and the nature and origin of the observed magnetic states.

An important issue in the context of transition metal oxides generally and *RENiO₃* materials in particular is orbital engineering: the degree to which the electronic structure and, in particular, the occupancy of different *d* orbitals and the number of bands crossing the Fermi level can be changed by strain or by heterostructuring (7). Following the proposal of Chaloupka and Khaliullin (109) that under appropriate circumstances LNO might exhibit a one-band Fermi surface analogous to that of the high- T_c cuprates, many groups (108, 116, 137) have investigated the degree to which orbital occupancies of *RENiO₃* materials can be manipulated. As far as is known, in bulk materials the relevant Ni *d* orbitals are roughly equally occupied. The key finding (67, 68, 107, 108, 113, 116) is that in strained SLs a differential orbital occupancy of up to 25% can be achieved. Understanding the limits of orbital engineering is a second challenge to theory.

We begin the theoretical discussion by consideration of the electronic configuration of Ni sites, which is a superposition of states with 6, 7, 8, or 9 Ni *d* electrons. We can schematically write

$$|\psi_{\text{Ni}}\rangle = \alpha|d^6\rangle + \beta|d^7\rangle + \gamma|d^8\rangle + \delta|d^9\rangle. \quad 2.$$

The Hund's and ligand field energies are such that the t_{2g} -symmetry *d* orbitals are fully filled and the relevant electronically active Ni *d* orbitals are the e_g states. Thus, d^6 corresponds to an empty Ni e_g shell, d^7 to an e_g shell with one electron, and so forth. Although the Hund's coupling, J_H , is evidently not strong enough to overcome the ligand field, it is believed to be strong enough to ensure that the dominant d^8 configuration is high spin ($S=1$, with one electron in each e_g orbital).

The nickelates are believed to be strongly correlated materials in which interaction effects beyond DFT play a key role in the physics. As a simple example, in DFT the occupation probabilities of the different Ni valences (squares of the coefficients in Equation 2) are determined by the mean occupancy and noninteracting electron statistics; in the actual materials the mean occupancy may be different from that predicted by DFT, and the relative probabilities of different states are likely to be strongly affected by interactions. However, results of DFT calculations and their $+U$ extensions

play an important role in our understanding of the materials, provide the only convenient mechanism for comprehensive structural relaxation, and are the starting point for beyond-DFT many-body calculations.

The basic picture emerging from standard DFT calculations is that the mean Ni d valence is slightly greater than 8 (112) and that in the ideal structure two bands, of mixed Ni e_g and O $2p$ origin, cross the Fermi level (in the actual materials, monoclinic or GdFeO₃-type distortions increase the unit cell so that it contains 4 Ni ions; the associated backfolding leads to multiple band crossings). Structural relaxation calculations indicate an increasing degree of GdFeO₃ distortion as the RE ion is changed from Nd across the series to Lu, consistent with experiment, and provide valuable information regarding rotational changes in SLs (94). Pure DFT calculations generally predict a metallic and nonmagnetic ground state in all members of the family.

The $+U$ extensions of DFT do find a charge-ordered ground state for reasonable values of U (138) but greatly overestimate the critical pressure required to destroy the charge ordering (139, 140). Jahn-Teller effects associated with lifting the degeneracy of the two e_g states were considered by He & Millis (141) and were found to become relevant at large ($\sim 4\%$) strains. In addition, the $+U$ methodologies predict a ferromagnetic ground state, rather than the long-period E or E' state observed experimentally. However, for a reasonable range of U , Bellaiche and coworkers (142) were able to stabilize the E' AFM state (two inequivalent Ni atoms: one associated with the long-bond octahedron and carrying a nonzero moment and the other associated with the short-bond octahedron and carrying zero moment) as a metastable state. Puggioni et al. (143) as well as Bruno et al. (71) used hybrid functional methods for strained films of the nickelates to show that the experimentally observed ground state is reproduced in these calculations.

An alternative family of theoretical approaches uses model calculations based on simple physical pictures following the assumption that, in the ground state, only one valence is dominant. The Mott-Hubbard picture is based on the assumption that the relevant valence is d^7 . In this picture, the main charge transfer process involves removing an electron from one site (creating a d^6 configuration) and adding it to an adjacent site, creating a d^8 configuration so that the key energy is $U = E(d^8) + E(d^6) - 2E(d^7)$. One expects $U > 0$, in which case the important physical effects are the Mott transition (conductivity is blocked if U is too large relative to the bandwidth) and Jahn-Teller physics associated with cubic-tetragonal distortions that lift the degeneracy of the d^7 state. Also important is J_H , which favors high-spin configurations.

To study this situation, one considers a Hubbard-like model, with two bands (representing the Ni e_g states or, in a more sophisticated interpretation, the e_g -O $2p$ antibonding bands) that are subject to U , J_H , and perhaps electron-phonon interaction. Several researchers have taken this approach (95, 96, 109, 110, 138). Mazin and coworkers (138) (using an approach based much more closely on DFT calculations) observed that, at the crossover between itinerant and localized behavior (with a bandwidth comparable to the Coulomb repulsion), interesting physics can occur; in particular, if the intra-atomic exchange interaction strength J_H is large enough, it may drive charge ordering.

Hansmann and collaborators (110) studied the Mott-Hubbard picture, using a DFT + DMFT methodology in which the correlated orbitals were built from the near Fermi surface e_g -derived conduction bands. They found that, for the generally accepted values of U and J_H the materials were near a Mott MIT. No indication of charge ordering was found. A SL-induced breaking of the cubic (O_h) point symmetry down to tetrahedral (T_d) was found to drive a very substantial orbital polarization, leading, for reasonable parameters, to a single-band Fermi surface.

Lee and coworkers (95, 96) addressed the weak-coupling physics of orbitally degenerate Mott-Hubbard systems by using a Hartree-Fock analysis of a two-band model with a band structure corresponding to the calculated near Fermi surface bands of LNO. A considerable degree of Fermi

surface nesting leads to a susceptibility $\chi(q)$ peaked close to the q value at which the magnetic ordering has been observed in experiments. Lee and coworkers noted that, for site-centered but not bond-centered spin-density waves, symmetry considerations imply that the magnetic ordering would also lead to charge ordering (with the amplitude of charge order proportional to the square of the magnetic order parameter), providing a possible theoretical explanation of PrNiO₃ and NNO for which the magnetic ordering and charge ordering coincide. However, this reasoning cannot be extended to those nickelates for which the magnetic ordering and MIT were separated unless unreasonably large values of J_H are assumed.

If Δ is positive and reasonably large (but less than U) and β (Equation 2) is still reasonably close to 1, one finds that the Mott-Hubbard picture provides a reasonable first-order description of the physics, with Δ playing the role of U . This picture yields, for example, the basic understanding of the high- T_c cuprates (144–146). However, in the *RE* nickelates, Δ may be negative, implying different physics. As noted above, DFT calculations indicate that the dominant electronic configuration is $d^8\bar{L}$ ($\gamma > \beta$) (112) and that Δ is negative. Mizokawa et al. (40) explored the potential relevance of the negative-charge-transfer-energy situation to nickelate physics in the context of a Hartree-Fock analysis of an extended Hubbard model that also included oxygen orbitals. In this situation, holes are present on the oxygen, and a purely electronic mechanism for insulating behavior requires ordering of the oxygen holes. Ordering of oxygen holes occurred only for extremely unphysically large magnitudes of charge transfer energy ($\Delta \lesssim -7\text{eV}$), so these authors concluded that the combination of breathing-mode distortions and strong correlations on the Ni site was essential for stabilizing the insulating state.

Marianetti, Millis & coworkers (112, 139, 140, 147) more quantitatively examined the negative-charge-transfer-energy scenario by using a DFT + DMFT methodology in which the correlated states were taken to be atomic-like Ni states constructed from Wannier functions defined over the full energy range of the Ni-O band complex and the O states were explicitly retained in the DMFT self-consistency equation. As with all beyond-DFT approaches, the results depend to some degree on the values chosen for the interaction parameters U and J and for the double-counting correction (145, 146, 148, 149). The important results summarized here do not depend on the precise values chosen.

The DFT + DMFT calculations lead to a mean d occupancy slightly smaller than the ~ 8.2 value found in DFT but still closer to 8 than to 7. One recent calculation found a mean value of ~ 7.8 , (139, 147), with $\alpha^2 = 0.24$, $\beta^2 = 0.22$, $\gamma^2 = 0.43$, and $\delta^2 = 0.11$ (H. Park, personal communication). The dominance of the d^8 state is characteristic of all DFT + DMFT calculations based on atomic-like Ni orbitals. Furthermore, the physically relevant values of the Hund's couplings, $J_H \sim 0.7\text{--}1$ eV, mean that the only d^8 state that occurs with appreciable probability is the high-spin d^8 state, in which each e_g orbital is occupied by one electron. This state is not susceptible to orbital polarization effects arising from strain or heterostructuring. In consequence, the orbital polarization is suppressed. The maximum polarization achievable under the strongest combinations of strain and heterostructuring is found to be $\sim 25\%$ (67, 68, 80, 107, 108, 113, 116), far too small to provide the one-band cuprate-like physics anticipated on the basis of the Mott-Hubbard-like calculations.

By solving the DFT + DMFT equations in the paramagnetic phase using the atomic positions appropriate for insulating LuNiO₃ in its ground state, Park and coworkers (147) found a novel insulating state, which may be termed either a site-selective Mott state or a hybridization wave insulator. In this state, the mean d valences of the two structurally inequivalent Ni sites were almost the same, corresponding to approximately two electrons in the e_g orbitals. On each site, the two electrons are correlated by the Hund's coupling into an $S = 1$ state. On the long-bond site, the $S = 1$ is decoupled from the environment, so the prediction is that, for example, an NMR

measurement in the paramagnetic state would reveal a freely fluctuating $S = 1$ local moment. On the other site, the $S = 1$ is strongly hybridized to the two holes on the O sites, leading to a singlet. The DFT + DMFT calculations provide an explicit realization of this state, which is insulating. As with other DFT+ methodologies, the DFT + DMFT methodology indicates a ferrimagnetic ground state, rather than the long-period AFM state observed experimentally. In the ferrimagnetic state, the moment size alternates: It is small on the short-bond site and large on the long-bond site. These conclusions were subsequently reproduced by Johnson et al. (150), who performed exact diagonalization studies of the one- and three-dimensional Ni-O clusters.

More recently, Park et al. (139, 140) performed total energy calculations within the DFT + DMFT methodology. By examining the variation of energy along a structural path interpolating from the cubic perovskite to the experimental LuNiO_3 structure, these authors showed that the DFT + DMFT methodology reproduces the salient features of the pressure- RE phase diagram of the materials, including the metallic nature of LNO and the critical pressures for the other compounds. DFT + U methods greatly overestimated the critical pressures.

These calculations establish a reasonably consistent physical picture of the nickelates as materials with a modestly negative charge transfer energy, far from the Mott-Hubbard limit but with strong correlations, only a modest susceptibility to orbital polarization, and an important coupling between electronic behavior and the lattice. The physics involves entangled Ni- d and O_{2p} states (with the entanglement crucially affected by the Hund's coupling). An interesting challenge for future research is to understand the consequences of this negative-charge-transfer physics for other aspects of the behavior of the nickelates, including the magnetic order, the quasiparticle properties of metallic states, and dynamical electron-lattice effects. In this regard, a very interesting step was taken by Subedi et al. (151), who argued that the low-energy physics of the negative-charge-transfer, Ni-O-entangled state may be represented by a negative U -positive J_{H} Hubbard model. Further exploration of this and other theoretical approaches seems highly desirable.

7. CONCLUDING REMARKS AND FUTURE ISSUES

With a brief introduction to the classification of electronic structure for correlated oxides, we review above the recent progress in the field of interface-controlled ground-state engineering of the $RE\text{NiO}_3$ series and the simultaneous development of theoretical understanding about the origin of transitions. The possibility of realizing high-temperature superconductivity through orbital engineering was the initial motivation for studying $RE\text{NiO}_3$ in ultrathin heterostructure form, and the consequent efforts to stabilize various artificial geometries with unit cell precession have allowed for the modulation of the ground states of the bulk phase diagram. Most importantly, this heterostructuring route has also resulted in several unconventional phases such as insulating states without charge order, NFL metallic phases, and antiferromagnetism in the metallic state, which are unattainable in the bulk. Here, we highlight several important issues for future consideration.

7.1. Exploration of Crystals Beyond Simple Perovskites

Although pushing synthesis of thin films of the highly distorted member of the series $RE = \text{Y, Dy, Ho} \dots \text{Lu}$ is an interesting avenue of research, other geometries of Ni coordination offer interesting possibilities for tuning the physical group states. As seen above, strained $RE\text{NiO}_3$ films result in rather small orbital polarization and are limited by the ability to distort NiO_6 octahedra in a highly connected perovskite network. One effective way to induce larger orbital polarization could be to move beyond simple perovskites into other classes of nickelates. One avenue involves layered nickelate phases in the Ruddlesden-Popper series (152, 153) and oxygen-reduced cuprate-like

variants, e.g., $\text{La}_3\text{Ni}_2\text{O}_6$ (154) and $\text{La}_4\text{Ni}_3\text{O}_8$ (155, 156). The large tetragonal distortion or absence of the apical oxygen in these compounds gives rise to strong variations in the crystal field that can be used to tune orbital energies. In this series, thin-film growth also offers opportunities to tune orbitals via cation ordering (157). Another option, ANiO_2 compounds such as LiNiO_2 that display interesting electronic and magnetic states (158, 159), remains largely unexplored from the perspective of epitaxial control.

7.2. Role of Oxygen in Electronic and Magnetic Transitions

Resonant X-ray absorption spectroscopy has firmly established the presence of holes on oxygen, and the theoretical studies have also emphasized the ordering of the ligand holes in a particular fashion across the transitions. Although checkerboard-type charge ordering and the E' magnetic structure of the Ni sublattice have been confirmed by resonant X-ray scattering in bulk, the ligand hole ordering and magnetism associated with the oxygen sublattice have not been experimentally verified due to limitations of scattering geometry. An experimental answer to these crucial issues can be the key to disentangling the puzzle of charge and E' magnetic ordering.

7.3. Ground-State Engineering Using External Stimuli

So far, this review focuses on metastable states created using different architectures during growth. In this section, we explore the opportunities to drive these systems nonadiabatically even further away from equilibrium via external driving forces, and we focus on two areas: optical control with visible and mid-IR sources and ionic control by applying strong electrochemical gradients. Both approaches have unique portions of phase space that can be accessed as described below.

7.3.1. Ultrafast dynamics in nickelate heterostructures. Stimulating phase changes using optical pulses is a well-established way to control ground states in complex oxides (160) and offers the ability to drive a system far off the equilibrium axis as a means to trigger phase transitions or seek out wholly new emergent states. Initial work on nickelates focused on tracking the time response of the carrier dynamics (29, 161) and coherent phonon excitation to probe the nature of electron-phonon coupling (162), but recently this approach was extended using ultrafast soft X-rays to track the response of magnetism to optical excitation (163). In NNO, the collapse of the AFM order as probed by resonant scattering at the AFM Bragg peak revealed an ultrafast collapse of the ordering of the Ni moments, followed by much slower dynamics for the parasitic magnetism related to low-temperature ordering of the Nd moments. Direct exploration of the magnetic order gives important insight into the interaction between the MIT and magnetism. However, the recovery process is much more difficult to understand due to the high energy of optical excitation; the system equilibrates on the longer timescale of several picoseconds due to heat generated during the carrier relaxation process via electron-lattice coupling.

To circumvent this issue, researchers have been exploring mode-selective excitations that can efficiently transfer the energy in the optical excitation to the system. One very intriguing approach demonstrated recently is the direct excitation of collective modes by light in the THz-to-mid-IR regime (160, 164, 165). This approach was first demonstrated in bulk complex oxides as a route to control the MIT by pumping specific phonon modes in the mid-IR that couple to the electronic degrees of freedom (166) and was later shown to be a way to dynamically control the superconducting phase in cuprates (167). Caviglia et al. (84) also applied this approach to nickelate films to control the MIT. The experiment demonstrated that, by pumping a substrate phonon mode that generated an ultrafast strain wave, the system could be converted to the metallic

phase (84). By merging mode-selective pumping with ultrafast soft-X-ray scattering, Caviglia and colleagues (168) were also able to measure the propagation of the phonon from the substrate into the film by following the spatial collapse of the magnetic state. This result confirmed that the nonlinear nature of the phonon excitation is a key component for triggering the transition (164). Very recently, a DMFT theoretical framework appeared to predict couplings to design materials for far more efficient dynamic control (169). In the future, this approach has the potential to offer new ways to efficiently manipulate correlated electron systems.

7.3.2. Ionic control. Another new control avenue for nickelates is through the use of electric fields applied to thin-film samples to manipulate carrier doping, analogous to gate control in semiconducting devices (170). Ionic liquids have emerged in this area as a means to apply large electric potentials through the use of a molecular electric double layer that forms on the surface of a sample. Although this approach was efficiently used to control the MIT in several systems (83, 171–176), the recent picture of charge carrier doping turned out to be more related to doping via the injection of oxygen vacancies under large applied electrochemical potential gradients (177, 178). Although the timescale of this method is much slower due to doping via ionic diffusion, this process offers the ability to change a material's phase through large stoichiometric changes that have not been available via gating in more conventional oxide devices (170). Recently, in another interesting approach, ionically gated *RE* nickelates were used to construct new classes of electronics based on neuromorphic (i.e., brain-like) principles (179, 180).

DISCLOSURE STATEMENT

The authors are not aware of any affiliations, memberships, funding, or financial holdings that might be perceived as affecting the objectivity of this review.

ACKNOWLEDGMENTS

The work is supported primarily by the Indo-US Joint Center for Rational Control of Functional Oxides under the Indo-US Science and Technology Forum. S.M. was supported by Department of Defense–Army Research Office grant 0402-17291, and J.C. was supported by the Gordon and Betty Moore Foundation EPiQS Initiative through grant GBMF4534. Work at the Advanced Photon Source is supported by the US Department of Energy, Office of Science, under grant DEAC02-06CH11357. We thank S. Stemmer, S. Ramanathan, A. Georges, G.A. Fiete, and D. Khomskii for insightful comments.

LITERATURE CITED

1. Imada M, Fujimori A, Tokura Y. 1998. Metal-insulator transitions. *Rev. Mod. Phys.* 70:1039–263
2. Zaanen J, Sawatzky GA, Allen JW. 1985. Band gaps and electronic structure of transition-metal compounds. *Phys. Rev. Lett.* 55:418–21
3. Nimkar S, Sarma DD, Krishnamurthy HR, Ramasesha S. 1993. Mean-field results of the multiple-band extended Hubbard model for the square-planar CuO₂ lattice. *Phys. Rev. B* 48:7355–63
4. Zubko P, Gariglio S, Gabay M, Ghosez P, Triscone JM. 2011. Interface physics in complex oxide heterostructures. *Annu. Rev. Condens. Matter Phys.* 2:141–65
5. Hwang HY, Iwasa Y, Kawasaki M, Keimer B, Nagaosa N, Tokura Y. 2012. Emergent phenomena at oxide interfaces. *Nat. Mater.* 11:103–13
6. Chakhalian J, Millis AJ, Rondinelli J. 2012. Whither the oxide interface. *Nat. Mater.* 11:92–94

7. Chakhalian J, Freeland JW, Millis AJ, Panagopoulos C, Rondinelli JM. 2014. Colloquium: Emergent properties in plane view: strong correlations at oxide interfaces. *Rev. Mod. Phys.* 86:1189–202
8. Bhattacharya A, May SJ. 2014. Magnetic oxide heterostructures. *Annu. Rev. Mater. Res.* 44:65–90
9. Slater JC. 1951. Magnetic effects and the Hartree-Fock equation. *Phys. Rev.* 82:538
10. Terakura K, Oguchi T, Williams AR, Kübler J. 1984. Band theory of insulating transition-metal monoxides: band-structure calculations. *Phys. Rev. B* 30:4734–47
11. Mott NF. 1949. The basis of the electron theory of metals, with special reference to the transition metals. *Proc. Phys. Soc. A* 62:416–22
12. Mott NF. 1961. The transition to the metallic state. *Philos. Mag.* 6:287–309
13. Hubbard J. 1963. Electron correlations in narrow energy bands. *Proc. R. Soc. A* 276:238–57
14. Hubbard J. 1964. Electron correlations in narrow energy bands. II. The degenerate band case. *Proc. R. Soc. A* 277:237–59
15. Fujimori A, Minami F. 1984. Valence-band photoemission and optical absorption in nickel compounds. *Phys. Rev. B* 30:957–71
16. Bandyopadhyay T, Sarma DD. 1989. Calculation of Coulomb interaction strengths for 3d transition metals and actinides. *Phys. Rev. B* 39:3517–21
17. Mahadevan P, Shanthi N, Sarma DD. 1996. Estimates of electronic interaction parameters for LaMO₃ compounds ($M = \text{Ti-Ni}$) from ab initio approaches. *Phys. Rev. B* 54:11199–206
18. Sarma D. 1990. Electronic structure of transition metal compounds: photoemission experiments and model Hamiltonian calculations. *J. Solid State Chem.* 88:45–52
19. Mizokawa T, Fujimori A, Namatame H, Akeyama K, Kosugi N. 1994. Electronic structure of the local-singlet insulator NaCuO₂. *Phys. Rev. B* 49:7193–204
20. Nimkar S, Sarma DD, Krishnamurthy HR. 1993. Electronic structure of NaCuO₂. *Phys. Rev. B* 47:10927–30
21. Sarma D, Krishnamurthy H, Nimkar S, Mitra PP, Ramasesha S, Ramakrishnan T. 1992. Electronic structure of the high- T_c cuprate superconductors and related compounds. *Pramana* 38:L531–38
22. Sarma D, Shanthi N, Mahadevan P. 1994. Electronic structure and the metal-insulator transition in LnNiO₃ (Ln = La, Pr, Nd, Sm and Ho): band structure results. *J. Phys. Condens. Matter* 6:10467
23. Barman SR, Chainani A, Sarma DD. 1994. Covalency-driven unusual metal-insulator transition in nickelates. *Phys. Rev. B* 49:8475–78
24. Sarma DD, Shanthi N, Barman SR, Hamada N, Sawada H, Terakura K. 1995. Band theory for ground-state properties and excitation spectra of perovskite LaMO₃ ($M = \text{Mn, Fe, Co, Ni}$). *Phys. Rev. Lett.* 75:1126–29
25. Medarde ML. 1997. Structural, magnetic and electronic properties of RNiO₃ perovskites ($R = \text{rare earth}$). *J. Phys. Condens. Matter* 9:1679
26. Catalan G. 2008. Progress in perovskite nickelate research. *Phase Transit.* 81:729–49
27. Ha SD, Jaramillo R, Silevitch DM, Schoofs F, Kerman K, et al. 2013. Hall effect measurements on epitaxial SmNiO₃ thin films and implications for antiferromagnetism. *Phys. Rev. B* 87:125150
28. Eguchi R, Chainani A, Taguchi M, Matsunami M, Ishida Y, et al. 2009. Fermi surfaces, electron-hole asymmetry, and correlation kink in a three-dimensional Fermi liquid LaNiO₃. *Phys. Rev. B* 79:115122
29. Katsufuji T, Okimoto Y, Arima T, Tokura Y, Torrance JB. 1995. Optical spectroscopy of the metal-insulator transition in NdNiO₃. *Phys. Rev. B* 51:4830–35
30. Catalan G, Bowman RM, Gregg JM. 2000. Metal-insulator transitions in NdNiO₃ thin films. *Phys. Rev. B* 62:7892–900
31. Allen SJ, Hauser AJ, Mikheev E, Zhang JY, Moreno NE, et al. 2015. Gaps and pseudogaps in perovskite rare earth nickelates. *APL Mater.* 3:062503
32. Scagnoli V, Staub U, Janousch M, Mulders AM, Shi M, et al. 2005. Charge disproportionation and search for orbital ordering in NdNiO₃ by use of resonant X-ray diffraction. *Phys. Rev. B* 72:155111
33. Scagnoli V, Staub U, Mulders AM, Janousch M, Meijer GI, et al. 2006. Role of magnetic and orbital ordering at the metal-insulator transition in NdNiO₃. *Phys. Rev. B* 73:100409
34. García-Muñoz JL, Rodríguez-Carvajal J, Lacorre P. 1994. Neutron-diffraction study of the magnetic ordering in the insulating regime of the perovskites RNiO₃ ($R = \text{Pr and Nd}$). *Phys. Rev. B* 50:978–92

35. Scagnoli V, Staub U, Bodenthin Y, García-Fernández M, Mulders AM, et al. 2008. Induced noncollinear magnetic order of Nd^{3+} in NdNiO_3 observed by resonant soft X-ray diffraction. *Phys. Rev. B* 77:115138
36. Alonso JA, García-Muñoz JL, Fernández-Díaz MT, Aranda MAG, Martínez-Lope MJ, Casais MT. 1999. Charge disproportionation in RNiO_3 perovskites: simultaneous metal-insulator and structural transition in YNiO_3 . *Phys. Rev. Lett.* 82:3871–74
37. Vobornik I, Perfetti L, Zacchigna M, Grioni M, Margaritondo G, et al. 1999. Electronic-structure evolution through the metal-insulator transition in RNiO_3 . *Phys. Rev. B* 60:R8426–29
38. Rodríguez-Carvajal J, Rosenkranz S, Medarde M, Lacorre P, Fernández-Díaz MT, et al. 1998. Neutron-diffraction study of the magnetic and orbital ordering in $^{154}\text{SmNiO}_3$ and $^{153}\text{EuNiO}_3$. *Phys. Rev. B* 57:456–64
39. Bodenthin Y, Staub U, Piamonteze C, García-Fernández M, Martínez-Lope MJ, Alonso JA. 2011. Magnetic and electronic properties of RNiO_3 ($\text{R} = \text{Pr, Nd, Eu, Ho}$ and Y) perovskites studied by resonant soft X-ray magnetic powder diffraction. *J. Phys. Condens. Matter* 23:036002
40. Mizokawa T, Khomskii DI, Sawatzky GA. 2000. Spin and charge ordering in self-doped Mott insulators. *Phys. Rev. B* 61:11263
41. Lacorre P, Torrance J, Pannetier J, Nazzari A, Wang P, Huang T. 1991. Synthesis, crystal structure, and properties of metallic PrNiO_3 : comparison with metallic NdNiO_3 and semiconducting SmNiO_3 . *J. Solid State Chem.* 91:225–37
42. Alonso JA, Muñoz A, Largeteau A, Demazeau G. 2004. Crystal growth of NdNiO_3 perovskite under high oxygen pressure. *J. Phys. Condens. Matter* 16:S1277–81
43. Prasad KVR, Varma KBR, Raju AR, Satyalakshmi KM, Mallya RM, Hegde MS. 1993. Growth and ferroelectric properties of $\text{Bi}_2\text{VO}_{5.5}$ thin films with metallic LaNiO_3 electrodes. *Appl. Phys. Lett.* 63:1898–900
44. Yang C, Chen M, Hong T, Wu C, Wu J, Wu T. 1995. Preparation of (100)-oriented metallic LaNiO_3 thin films on Si substrates by radio frequency magnetron sputtering for the growth of textured $\text{Pb}(\text{Zr}_{0.53}\text{Ti}_{0.47})\text{O}_3$. *Appl. Phys. Lett.* 66:2643
45. DeNatale JF, Kobrin PH. 1996. Lattice distortion effects on electrical switching in epitaxial thin film NdNiO_3 . *J. Mater. Res.* 12:2992–95
46. Novojilov MA, Gorbenco OY, Graboy IE, Kaul AR, Zandbergen HW, et al. 2000. Perovskite rare-earth nickelates in the thin-film epitaxial state. *Appl. Phys. Lett.* 76:2041–43
47. Catalan G, Bowman RM, Gregg JM. 2000. Transport properties of NdNiO_3 thin films made by pulsed-laser deposition. *J. Appl. Phys.* 87:606–8
48. Son J, Moetakef P, LeBeau JM, Ouellette D, Balents L, et al. 2010. Low-dimensional Mott material: transport in ultrathin epitaxial LaNiO_3 films. *Appl. Phys. Lett.* 96:062114
49. Nikolaev KR, Bhattacharya A, Kraus PA, Vas'ko VA, Cooley WK, Goldman AM. 1999. Indications of antiferromagnetic interlayer coupling in $\text{La}_{2/3}\text{Ba}_{1/3}\text{MnO}_3/\text{LaNiO}_3$ multilayers. *Appl. Phys. Lett.* 75:118–20
50. Kaul AR, Gorbenco OY, Kamenev AA. 2004. The role of heteroepitaxy in the development of new thin-film oxide-based functional materials. *Russ. Chem. Rev.* 73:861
51. Gorbenco OY, Samoilencov S, Graboy I, Kaul A. 2002. Epitaxial stabilization of oxides in thin films. *Chem. Mater.* 14:4026–43
52. Chen J, Zhou Y, Middey S, Jiang J, Chen N, et al. 2015. Self-limited kinetics of electron doping in correlated oxides. *Appl. Phys. Lett.* 107:031905
53. Ha SD, Otaki M, Jaramillo R, Podpirka A, Ramanathan S. 2012. Stable metal-insulator transition in epitaxial SmNiO_3 thin films. *J. Solid State Chem.* 190:233–37
54. Kareev M, Prosandeev S, Gray B, Liu J, Ryan P, et al. 2011. Sub-monolayer nucleation and growth of complex oxides at high supersaturation and rapid flux modulation. *J. Appl. Phys.* 109:114303
55. Feigl L, Schultz B, Ohya S, Ouellette D, Kozhanov A, Palmstram C. 2013. Structural and transport properties of epitaxial PrNiO_3 thin films grown by molecular beam epitaxy. *J. Cryst. Growth* 366:51–54
56. Liu J, Kareev M, Gray B, Kim JW, Ryan P, et al. 2010. Strain-mediated metal-insulator transition in epitaxial ultrathin films of NdNiO_3 . *Appl. Phys. Lett.* 96:233110
57. Meyers D, Moon EJ, Kareev M, Tung I, Gray BA, et al. 2013. Epitaxial stabilization of ultra-thin films of EuNiO_3 . *J. Phys. D* 46:385303

58. Hauser AJ, Mikheev E, Moreno NE, Hwang J, Zhang JY, Stemmer S. 2015. Correlation between stoichiometry, strain, and metal-insulator transitions of NdNiO₃ films. *Appl. Phys. Lett.* 106:092104
59. Jaramillo R, Schoofs F, Ha SD, Ramanathan R. 2013. High pressure synthesis of SmNiO₃ thin films and implications for thermodynamics of the nickelates. *J. Mater. Chem. C* 1:2455
60. Bristowe NC, Ghosez P, Littlewood PB, Artacho E. 2014. The origin of two-dimensional electron gases at oxide interfaces: insights from theory. *J. Phys. Condens. Matter* 26:143201
61. Liu J, Kareev M, Prosandeev S, Gray B, Ryan P, et al. 2010. Effect of polar discontinuity on the growth of LaNiO₃/LaAlO₃ superlattices. *Appl. Phys. Lett.* 96:133111
62. Detemple E, Ramasse QM, Sigle W, Cristiani G, Habermeier HU, et al. 2011. Polarity-driven nickel oxide precipitation in LaNiO₃-LaAlO₃ superlattices. *Appl. Phys. Lett.* 99:211903
63. Rondinelli JM, May SJ, Freeland JW. 2012. Control of octahedral connectivity in perovskite oxide heterostructures: an emerging route to multifunctional materials discovery. *MRS Bull.* 37:261–70
64. Moon EJ, Gray BA, Kareev M, Liu J, Altendorf SG, et al. 2011. Strain-dependent transport properties of the ultra-thin correlated metal, LaNiO₃. *New J. Phys.* 13:073037
65. Moon EJ, Rondinelli JM, Prasai N, Gray BA, Kareev M, et al. 2012. Strain-controlled band engineering and self-doping in ultrathin LaNiO₃ films. *Phys. Rev. B* 85:121106
66. May SJ, Kim JW, Rondinelli JM, Karapetrova E, Spaldin NA, et al. 2010. Quantifying octahedral rotations in strained perovskite oxide films. *Phys. Rev. B* 82:014110
67. Tung IC, Balachandran PV, Liu J, Gray BA, Karapetrova EA, et al. 2013. Connecting bulk symmetry and orbital polarization in strained RNiO₃ ultrathin films. *Phys. Rev. B* 88:205112
68. Chakhalian J, Rondinelli JM, Liu J, Gray BA, Kareev M, et al. 2011. Asymmetric orbital-lattice interactions in ultrathin correlated oxide films. *Phys. Rev. Lett.* 107:116805
69. Liu J, Kargarian M, Kareev M, Gray B, Ryan PJ, et al. 2013. Heterointerface engineered electronic and magnetic phases of NdNiO₃ thin films. *Nat. Commun.* 4:2714
70. Meyers D, Middey S, Kareev M, van Veenendaal M, Moon EJ, et al. 2013. Strain-modulated Mott transition in EuNiO₃ ultrathin films. *Phys. Rev. B* 88:075116
71. Bruno FY, Rushchanskii KZ, Valencia S, Dumont Y, Carrétéro C, et al. 2013. Rationalizing strain engineering effects in rare-earth nickelates. *Phys. Rev. B* 88:195108
72. Hepting M, Minola M, Frano A, Cristiani G, Logvenov G, et al. 2014. Tunable charge and spin order in PrNiO₃ thin films and superlattices. *Phys. Rev. Lett.* 113:227206
73. Catalano S, Gibert M, Bisogni V, Peil OE, He F, et al. 2014. Electronic transitions in strained SmNiO₃ thin films. *APL Mater.* 2:116110
74. Yoo HK, Hyun SI, Moreschini L, Kim HD, Chang YJ, et al. 2015. Latent instabilities in metallic LaNiO₃ films by strain control of Fermi-surface topology. *Sci. Rep.* 5:8746
75. King PDC, Wei HI, Nie YF, Uchida M, Adamo C, et al. 2014. Atomic-scale control of competing electronic phases in ultrathin LaNiO₃. *Nat. Nanotechnol.* 9:443–47
76. Stewart MK, Liu J, Kareev M, Chakhalian J, Basov DN. 2011. Mott physics near the insulator-to-metal transition in NdNiO₃. *Phys. Rev. Lett.* 107:176401
77. Stewart MK, Yee CH, Liu J, Kareev M, Smith RK, et al. 2011. Optical study of strained ultrathin films of strongly correlated LaNiO₃. *Phys. Rev. B* 83:075125
78. Stewart MK, Brownstead D, Liu J, Kareev M, Chakhalian J, Basov DN. 2012. Heterostructuring and strain effects on the infrared optical properties of nickelates. *Phys. Rev. B* 86:205102
79. Tebano A, Aruta C, Sanna S, Medaglia PG, Balestrino G, et al. 2008. Evidence of orbital reconstruction at interfaces in ultrathin La_{0.67} Sr_{0.33} MnO₃ films. *Phys. Rev. Lett.* 100:137401
80. Peil OE, Ferrero M, Georges A. 2014. Orbital polarization in strained LaNiO₃: structural distortions and correlation effects. *Phys. Rev. B* 90:045128
81. Upton MH, Choi Y, Park H, Liu J, Meyers D, et al. 2015. Novel electronic behavior driving NdNiO₃ metal-insulator transition. *Phys. Rev. Lett.* 115:036401
82. Sarma DD, Shanthi N, Mahadevan P. 1996. Electronic excitation spectra from ab initio band-structure results for LaMO₃ (M = Cr, Mn, Fe, Co, Ni). *Phys. Rev. B* 54:1622–28
83. Scherwitzl R, Zubko P, Lezama IG, Ono S, Morpurgo AF, et al. 2010. Electric-field control of the metal-insulator transition in ultrathin NdNiO₃ films. *Adv. Mater.* 22:5517–20

84. Caviglia AD, Scherwitzl R, Popovich P, Hu W, Bromberger H, et al. 2012. Ultrafast strain engineering in complex oxide heterostructures. *Phys. Rev. Lett.* 108:136801
85. Hauser AJ, Mikheev E, Moreno NE, Cain TA, Hwang J, et al. 2013. Temperature-dependence of the Hall coefficient of NdNiO₃ thin films. *Appl. Phys. Lett.* 103:182105
86. Mikheev E, Hauser AJ, Himmetoglu B, Moreno NE, Janotti A, et al. 2015. Tuning bad metal and non-Fermi liquid behavior in a Mott material: rare earth nickelate thin films. *Sci. Adv.* 1:e1500797
87. Zhou JS, Goodenough JB, Dabrowski B. 2005. Pressure-induced non-Fermi-liquid behavior of PrNiO₃. *Phys. Rev. Lett.* 94:226602
88. Kobayashi H, Ikeda S, Yoda Y, Hirao N, Ohishi Y, et al. 2015. Pressure-induced unusual metallic state in EuNiO₃. *Phys. Rev. B* 91:195148
89. Jaramillo R, Ha SD, Silevitch DM, Ramanathan S. 2014. Origins of bad-metal conductivity and the insulator-metal transition in the rare-earth nickelates. *Nat. Phys.* 10:304–7
90. Meyers D, Liu J, Freeland JW, Middey S, Kareev M, et al. 2015. Selective interface control of order parameters in complex oxides. arXiv:1505.07451 [cond-mat.str-el]
91. Staub U, Meijer GL, Fauth F, Allenspach R, Bednorz JG, et al. 2002. Direct observation of charge order in an epitaxial NdNiO₃ film. *Phys. Rev. Lett.* 88:126402
92. Lorenzo JE, Hodeau JL, Paolasini L, Lefloch S, Alonso JA, Demazeau G. 2005. Resonant X-ray scattering experiments on electronic orderings in NdNiO₃ single crystals. *Phys. Rev. B* 71:045128
93. Meyers D, Middey S, Kareev M, Liu J, Kim JW, et al. 2015. Charge order and antiferromagnetism in epitaxial ultrathin films of EuNiO₃. *Phys. Rev. B* 92:235126
94. Balachandran PV, Rondinelli JM. 2013. Interplay of octahedral rotations and breathing distortions in charge-ordering perovskite oxides. *Phys. Rev. B* 88:054101
95. Lee SB, Chen R, Balents L. 2011. Landau theory of charge and spin ordering in the nickelates. *Phys. Rev. Lett.* 106:016405
96. Lee SB, Chen R, Balents L. 2011. Metal-insulator transition in a two-band model for the perovskite nickelates. *Phys. Rev. B* 84:165119
97. Scherwitzl R, Gariglio S, Gabay M, Zubko P, Gibert M, Triscone JM. 2011. Metal-insulator transition in ultrathin LaNiO₃ films. *Phys. Rev. Lett.* 106:246403
98. Liu J, Okamoto S, van Veenendaal M, Kareev M, Gray B, et al. 2011. Quantum confinement of Mott electrons in ultrathin LaNiO₃/LaAlO₃ superlattices. *Phys. Rev. B* 83:161102
99. Boris AV, Matiks Y, Benckiser E, Frano A, Popovich P, et al. 2011. Dimensionality control of electronic phase transitions in nickel-oxide superlattices. *Science* 332:937–40
100. Sakai E, Tamamitsu M, Yoshimatsu K, Okamoto S, Horiba K, et al. 2013. Gradual localization of Ni 3d states in LaNiO₃ ultrathin films induced by dimensional crossover. *Phys. Rev. B* 87:075132
101. Kumah DP, Disa AS, Ngai JH, Chen H, Malashevich A, et al. 2014. Tuning the structure of nickelates to achieve two-dimensional electron conduction. *Adv. Mater.* 26:1935–40
102. Gray AX, Janotti A, Son J, LeBeau JM, Ueda S, et al. 2011. Insulating state of ultrathin epitaxial LaNiO₃ thin films detected by hard X-ray photoemission. *Phys. Rev. B* 84:075104
103. Kaiser AM, Gray AX, Conti G, Son J, Greer A, et al. 2011. Suppression of near-Fermi level electronic states at the interface in a LaNiO₃/(SrTiO₃) superlattice. *Phys. Rev. Lett.* 107:116402
104. Hwang J, Son J, Zhang JY, Janotti A, Van de Walle CG, Stemmer S. 2013. Structural origins of the properties of rare earth nickelate superlattices. *Phys. Rev. B* 87:060101
105. Frano A, Schierle E, Haverkort MW, Lu Y, Wu M, et al. 2013. Orbital control of noncollinear magnetic order in nickel oxide heterostructures. *Phys. Rev. Lett.* 111:106804
106. Berner G, Sing M, Pfaff F, Benckiser E, Wu M, et al. 2015. Dimensionality-tuned electronic structure of nickelate superlattices explored by soft-X-ray angle-resolved photoelectron spectroscopy. *Phys. Rev. B* 92:125130
107. Benckiser E, Haverkort MW, Brück S, Goering E, Macke S, et al. 2011. Orbital reflectometry of oxide heterostructures. *Nat. Mater.* 10:189–93
108. Wu M, Benckiser E, Haverkort MW, Frano A, Lu Y, et al. 2013. Strain and composition dependence of orbital polarization in nickel oxide superlattices. *Phys. Rev. B* 88:125124
109. Chaloupka J, Khaliullin G. 2008. Orbital order and possible superconductivity in LaNiO₃/LaMO₃ superlattices. *Phys. Rev. Lett.* 100:016404

110. Hansmann P, Yang X, Toschi A, Khaliullin G, Andersen OK, Held K. 2009. Turning a nickelate Fermi surface into a cupratelike one through heterostructuring. *Phys. Rev. Lett.* 103:016401
111. Han MJ, Marianetti CA, Millis AJ. 2010. Chemical control of orbital polarization in artificially structured transition-metal oxides: La_2NiXO_6 ($X = \text{B, Al, Ga, In}$) from first principles. *Phys. Rev. B* 82:134408
112. Han MJ, Wang X, Marianetti CA, Millis AJ. 2011. Dynamical mean-field theory of nickelate superlattices. *Phys. Rev. Lett.* 107:206804
113. Freeland JW, Liu J, Kareev M, Gray B, Kim JW, et al. 2011. Orbital control in strained ultra-thin $\text{LaNiO}_3/\text{LaAlO}_3$ superlattices. *Europhys. Lett.* 96:57004
114. Disa AS, Kumah DP, Malashevich A, Chen H, Arena DA, et al. 2015. Orbital engineering in symmetry-breaking polar heterostructures. *Phys. Rev. Lett.* 114:026801
115. Blanca-Romero A, Pentcheva R. 2011. Confinement-induced metal-to-insulator transition in strained $\text{LaNiO}_3/\text{LaAlO}_3$ superlattices. *Phys. Rev. B* 84:195450
116. Wu M, Benckiser E, Audehm P, Goering E, Wochner P, et al. 2015. Orbital reflectometry of $\text{PrNiO}_3/\text{PrAlO}_3$ superlattices. *Phys. Rev. B* 91:195130
117. May SJ, Santos TS, Bhattacharya A. 2009. Onset of metallic behavior in strained $(\text{LaNiO}_3)_n/(\text{SrMnO}_3)_2$ superlattices. *Phys. Rev. B* 79:115127
118. Gibert M, Zubko P, Scherwitsl R, Íñiguez J, Triscone JM. 2012. Exchange bias in LaNiO_3 - LaMnO_3 superlattices. *Nat. Mater.* 11:195–98
119. Hoffman J, Tung IC, Nelson-Cheeseman BB, Liu M, Freeland JW, Bhattacharya A. 2013. Charge transfer and interfacial magnetism in $(\text{LaNiO}_3)_n/(\text{LaMnO}_3)_2$ superlattices. *Phys. Rev. B* 88:144411
120. Grutter AJ, Yang H, Kirby BJ, Fitzsimmons MR, Aguiar JA, et al. 2013. Interfacial ferromagnetism in $\text{LaNiO}_3/\text{CaMnO}_3$ superlattices. *Phys. Rev. Lett.* 111:087202
121. Di Pietro P, Hoffman J, Bhattacharya A, Lupi S, Perucchi A. 2015. Spectral weight redistribution in $(\text{LaNiO}_3)_n/(\text{LaMnO}_3)_2$ superlattices from optical spectroscopy. *Phys. Rev. Lett.* 114:156801
122. Piamonteze C, Gibert M, Heidler J, Dreiser J, Rusponi S, et al. 2015. Interfacial properties of $\text{LaMnO}_3/\text{LaNiO}_3$ superlattices grown along (001) and (111) orientations. *Phys. Rev. B* 92:014426
123. Chen H, Millis AJ, Marianetti CA. 2013. Engineering correlation effects via artificially designed oxide superlattices. *Phys. Rev. Lett.* 111:116403
124. Cao Y, Liu X, Kareev M, Choudhury D, Middey S, et al. 2016. Engineered Mott ground state in a $\text{LaTiO}_{3+\delta}/\text{LaNiO}_3$ heterostructure. *Nat. Commun.* 7:10418
125. Hoffman J, Kirby BJ, Kwon J, Freeland JW, Martin I, et al. 2014. Oscillatory non-collinear magnetism induced by interfacial charge transfer in metallic oxide superlattices. arXiv:1411.4344 [cond-mat.mtrl-sci]
126. Chen H, Kumah DP, Disa AS, Walker FJ, Ahn CH, Ismail-Beigi S. 2013. Modifying the electronic orbitals of nickelate heterostructures via structural distortions. *Phys. Rev. Lett.* 110:186402
127. Xiao D, Zhu W, Ran Y, Nagaosa N, Okamoto S. 2011. Interface engineering of quantum Hall effects in digital transition metal oxide heterostructures. *Nat. Commun.* 2:596
128. Rüegg A, Fiete GA. 2011. Topological insulators from complex orbital order in transition-metal oxides heterostructures. *Phys. Rev. B* 84:201103
129. Yang KY, Zhu W, Xiao D, Okamoto S, Wang Z, Ran Y. 2011. Possible interaction-driven topological phases in (111) bilayers of LaNiO_3 . *Phys. Rev. B* 84:201104
130. Wang F, Ran Y. 2011. Nearly flat band with Chern number $C = 2$ on the dice lattice. *Phys. Rev. B* 84:241103
131. Rüegg A, Mitra C, Demkov AA, Fiete GA. 2012. Electronic structure of $(\text{LaNiO}_3)_2/(\text{LaAlO}_3)_N$ heterostructures grown along [111]. *Phys. Rev. B* 85:245131
132. Rüegg A, Mitra C, Demkov AA, Fiete GA. 2013. Lattice distortion effects on topological phases in $(\text{LaNiO}_3)_2/(\text{LaAlO}_3)_N$ heterostructures grown along the [111] direction. *Phys. Rev. B* 88:115146
133. Doennig D, Pickett WE, Pentcheva R. 2014. Confinement-driven transitions between topological and Mott phases in $(\text{LaNiO}_3)_N/(\text{LaAlO}_3)_M$ (111) superlattices. *Phys. Rev. B* 89:121110
134. Middey S, Rivero P, Meyers D, Kareev M, Liu X, et al. 2014. Polarity compensation in ultra-thin films of complex oxides: the case of a perovskite nickelate. *Sci. Rep.* 4:6819
135. Middey S, Meyers D, Kareev M, Moon EJ, Gray BA, et al. 2012. Epitaxial growth of (111)-oriented $\text{LaAlO}_3/\text{LaNiO}_3$ ultra-thin superlattices. *Appl. Phys. Lett.* 101:261602

136. Middey S, Meyers D, Doennig D, Kareev M, Liu X, et al. 2016. Mott electrons in an artificial graphenelike crystal of rare-earth nickelate. *Phys. Rev. Lett.* 116:056801
137. Kinyanjui MK, Lu Y, Gauquelin N, Wu M, Frano A, et al. 2014. Lattice distortions and octahedral rotations in epitaxially strained $\text{LaNiO}_3/\text{LaAlO}_3$ superlattices. *Appl. Phys. Lett.* 104:221909
138. Mazin II, Khomskii DI, Lengsdorf R, Alonso JA, Marshall WG, et al. 2007. Charge ordering as alternative to Jahn-Teller distortion. *Phys. Rev. Lett.* 98:176406
139. Park H, Millis AJ, Marianetti CA. 2014. Total energy calculations using DFT + DMFT: computing the pressure phase diagram of the rare earth nickelates. *Phys. Rev. B* 89:245133
140. Park H, Millis AJ, Marianetti CA. 2014. Computing total energies in complex materials using charge self-consistent DFT + DMFT. *Phys. Rev. B* 90:235103
141. He Z, Millis AJ. 2015. Strain control of electronic phase in rare earth nickelates. *Phys. Rev. B* 91:195138
142. Prosandeev S, Bellaiche L, Iniguez J. 2012. Ab initio study of the factors affecting the ground state of rare-earth nickelates. *Phys. Rev. B* 85:214431
143. Puggioni D, Filippetti A, Fiorentini V. 2012. Ordering and multiple phase transitions in ultrathin nickelate superlattices. *Phys. Rev. B* 86:195132
144. Zhang FC, Rice TM. 1988. Effective Hamiltonian for the superconducting Cu oxides. *Phys. Rev. B* 37:3759–61
145. de' Medici L, Wang X, Capone M, Millis AJ. 2009. Correlation strength, gaps, and particle-hole asymmetry in high- T_c cuprates: a dynamical mean field study of the three-band copper-oxide model. *Phys. Rev. B* 80:054501
146. Wang X, de' Medici L, Millis AJ. 2011. Role of oxygen-oxygen hopping in the three-band copper-oxide model: quasiparticle weight, metal insulator and magnetic phase boundaries, gap values and optical conductivity. *Phys. Rev. B* 83:094501
147. Park H, Millis AJ, Marianetti CA. 2012. Site-selective Mott transition in rare-earth-element nickelates. *Phys. Rev. Lett.* 109:156402
148. Liechtenstein AI, Anisimov VI, Zaanen J. 1995. Density-functional theory and strong interactions: orbital ordering in Mott-Hubbard insulators. *Phys. Rev. B* 52:R5467–70
149. Karolak M, Ulm G, Wehling T, Mazurenko V, Poteryaev A, Lichtenstein A. 2010. Double counting in LDA plus DMFT—the example of NiO. *J. Electron Spectrosc. Relat. Phenom.* 181:11–15
150. Johnston S, Mukherjee A, Elfimov I, Berciu M, Sawatzky GA. 2014. Charge disproportionation without charge transfer in the rare-earth-element nickelates as a possible mechanism for the metal-insulator transition. *Phys. Rev. Lett.* 112:106404
151. Subedi A, Peil OE, Georges A. 2015. Low-energy description of the metal-insulator transition in the rare-earth nickelates. *Phys. Rev. B* 91:075128
152. Zhang Z, Greenblatt M, Goodenough J. 1994. Synthesis, structure, and properties of the layered perovskite $\text{La}_3\text{Ni}_2\text{O}_{7-\delta}$. *J. Solid State Chem.* 108:402
153. Yoshizawa H, Kakeshita T, Kajimoto R, Tanabe T, Katsufuji T, Tokura Y. 2000. Stripe order at low temperatures in $\text{La}_{2-x}\text{Sr}_x\text{NiO}_4$ with $0.289 < x < 0.5$. *Phys. Rev. B* 61:R854–57
154. Poltavets VV, Greenblatt M, Fecher GH, Felser C. 2009. Electronic properties, band structure, and Fermi surface instabilities of $\text{Ni}^{1+}/\text{Ni}^{2+}$ nickelate $\text{La}_3\text{Ni}_2\text{O}_6$, isoelectronic with superconducting cuprates. *Phys. Rev. Lett.* 102:046405
155. Poltavets VV, Lokshin KA, Nevidomskyy AH, Croft M, Tyson TA, et al. 2010. Bulk magnetic order in a two-dimensional $\text{Ni}^{1+}/\text{Ni}^{2+}$ (d^9/d^8) nickelate, isoelectronic with superconducting cuprates. *Phys. Rev. Lett.* 104:206403
156. Cheng JG, Zhou JS, Goodenough JB, Zhou HD, Matsubayashi K, et al. 2012. Pressure effect on the structural transition and suppression of the high-spin state in the triple-layer T' - $\text{La}_4\text{Ni}_3\text{O}_8$. *Phys. Rev. Lett.* 108:236403
157. Nelson-Cheeseman BB, Zhou H, Balachandran PV, Fabbris G, Hoffman J, et al. 2014. Polar cation ordering: a route to introducing > 10% bond strain into layered oxide films. *Adv. Funct. Mater.* 24:6884–91
158. Reynaud F, Mertz D, Celestini F, Debierre JM, Ghorayeb AM, et al. 2001. Orbital frustration at the origin of the magnetic behavior in LiNiO_2 . *Phys. Rev. Lett.* 86:3638–41

159. Kang JS, Lee SS, Kim G, Lee HJ, Song HK, et al. 2007. Valence and spin states in delafossite AgNiO_2 and the frustrated Jahn-Teller system ANiO_2 ($A = \text{Li, Na}$). *Phys. Rev. B* 76:195122
160. Zhang J, Averitt RD. 2014. Dynamics and control in complex transition metal oxides. *Annu. Rev. Mater. Res.* 44:19–43
161. Ruello P, Zhang S, Laffez P, Perrin B, Gusev V. 2007. Ultrafast electronic dynamics in the metal-insulator transition compound NdNiO_3 . *Phys. Rev. B* 76:165107
162. Ruello P, Zhang S, Laffez P, Perrin B, Gusev V. 2009. Laser-induced coherent acoustical phonons mechanisms in the metal-insulator transition compound NdNiO_3 : thermal and nonthermal processes. *Phys. Rev. B* 79:094303
163. Caviglia AD, Först M, Scherwitzl R, Khanna V, Bromberger H, et al. 2013. Photoinduced melting of magnetic order in the correlated electron insulator NdNiO_3 . *Phys. Rev. B* 88:220401
164. Först M, Manzoni C, Kaiser S, Tomioka Y, Tokura Y, et al. 2011. Nonlinear phononics as an ultrafast route to lattice control. *Nat. Phys.* 7:854
165. Kampfrath T, Tanaka K, Nelson KA. 2013. Resonant and nonresonant control over matter and light by intense terahertz transients. *Nat. Photonics* 7:680
166. Rini M, Tobey R, Dean N, Itatani J, Tomioka Y, et al. 2007. Control of the electronic phase of a manganite by mode-selective vibrational excitation. *Nature* 449:72–74
167. Fausti D, Tobey RI, Dean N, Kaiser S, Dienst A, et al. 2011. Light-induced superconductivity in a stripe-ordered cuprate. *Science* 331:189–91
168. Först M, Caviglia AD, Scherwitzl R, Mankowsky R, Zubko P, et al. 2015. Spatially resolved ultrafast magnetic dynamics initiated at a complex oxide heterointerface. *Nat. Mater.* 14:883–88
169. Subedi A, Cavalleri A, Georges A. 2014. Theory of nonlinear phononics for coherent light control of solids. *Phys. Rev. B* 89:220301
170. Ahn CH, Di Ventra M, Eckstein JN, Frisbie CD, Gershenson ME, et al. 2006. Electrostatic modification of novel materials. *Rev. Mod. Phys.* 78:1185–212
171. Ueno K, Shimotani H, Iwasa Y, Kawasaki M. 2010. Electrostatic charge accumulation versus electrochemical doping in SrTiO_3 electric double layer transistors. *Appl. Phys. Lett.* 96:252107
172. Asanuma S, Xiang PH, Yamada H, Sato H, Inoue IH, et al. 2010. Tuning of the metal-insulator transition in electrolyte-gated NdNiO_3 thin films. *Appl. Phys. Lett.* 97:142110
173. Nakano M, Shibuya K, Okuyama D, Hatano T, Ono S, et al. 2012. Collective bulk carrier delocalization driven by electrostatic surface charge accumulation. *Nature* 487:459–62
174. Shi J, Zhou Y, Ramanathan S. 2014. Colossal resistance switching and band gap modulation in a perovskite nickelate by electron doping. *Nat. Commun.* 5:4860
175. Ha SD, Vetter U, Shi J, Ramanathan S. 2013. Electrostatic gating of metallic and insulating phases in SmNiO_3 ultrathin films. *Appl. Phys. Lett.* 102:183102
176. Bubel S, Hauser AJ, Glaudell AM, Mates TE, Stemmer S, Chabiny ML. 2015. The electrochemical impact on electrostatic modulation of the metal-insulator transition in nickelates. *Appl. Phys. Lett.* 106:122102
177. Yang Z, Zhou Y, Ramanathan S. 2012. Studies on room-temperature electric-field effect in ionic-liquid gated VO_2 three-terminal devices. *J. Appl. Phys.* 111:014506
178. Jeong J, Aetukuri N, Graf T, Schladt TD, Samant MG, Parkin SSP. 2013. Suppression of metal-insulator transition in VO_2 by electric field-induced oxygen vacancy formation. *Science* 339:1402–5
179. Shi J, Ha SD, Zhou Y, Schoofs F, Ramanathan S. 2013. A correlated nickelate synaptic transistor. *Nat. Commun.* 4:2676
180. Ha S, Shi J, Meroz Y, Mahadevan L, Ramanathan S. 2014. Neuromimetic circuits with synaptic devices based on strongly correlated electron systems. *Phys. Rev. Appl.* 2:64003